Reviewer 2

We would like to sincerely thank the reviewer for his comments. We believe they help us to improve the manuscript significantly and give us many useful suggestions to improve the mission. We have corrected the manuscript according reviewer's comments and answer the reviewer's question point by point below.

Reviewer comments are in italic blue, the manuscript modifications are in red. The answer "Done" means that the manuscript has been modified following exactly the reviewer comment.

Reply to Minor comments

Abstract

A sentence on the comparison with AURA/MLS should be added in the abstract.

Reply: Done. A sentence has been added:

"A theoretical simulation is performed to estimate the retrieval precision of the main targets and to compare them with that of Aura MLS standard spectrometers"

P2 L17: "other abundant chemical species" -> "other trace chemical species"

Reply: Done.

P3P8: "5.5, 3.8, 3.3, and 0.96 km, respectively." -> "5.5, 3.8, 3.3, and 0.96 km at 118, 190, 240, 640 GHz, respectively."

Reply: Done.

*Table 1: Since there is an angle offset between the radiometers, how are defined the LOS angles? I have trouble to understand the relationship "0.1 s integration time -> 1 km tangent height spacing". If the total time for scanning from 0 to 100 km is 28 sec (36 - 5-3), 0.1 sec should be 0.35 km (100/28.*0.1). Do I misunderstand something?*

Reply: The LOS angle is the same, but there exists sequence between the radiometers. For example, 118 Ghz will scan the surface firstly, then 643 GHz will scan it, 190 GHz is the last. All the data will be recorded after 118 GHz start to work, so it has no impact on observation.

The total time of 36 second defined in paper includes a scan and retrace (retrace also records data, it will spend 18 second), for one single scan it is 18 second, so the time used to scan from 0-100 km is 10 seconds.

P5L9-10: I would recommend the authors to add the MLS reference on the 118 GHz line processing since their analysis of

this line is not complete (e.g., Zeeman effect). [Schwartz et al., EOS MLS forward model polarized radiative transfer for Zeeman-split oxygen, IEEE Transactions on Geoscience and Remote Sensing, doi:10.1109/TGRS.2005.862267]

Reply: Done. A sentence has been added:

"In addition, the Zeeman effect will affect the O_2 line, the influence should be studied (Schwartz et al, 2006)"

P6: A reference with MLS HCl could be added. For example: Lary, D.J., O. Aulov, "Space-based measurements of HCl: Intercomparison and historical context", Journal of Geophysical Research 113, D15S04, doi:10.1029/2007JD008715, 2008

Reply: Done.

P11L8, The reference given by the authors in their answer to my first review (referee 2) should be given ("Skou N, Vine D L.: Microwave Radiometer Systems: Design and Analysis, Norwood Ma Artech House P, 2006, 26-27"). Also the fact that the noise equivalent bandwidth of a DSB receiver is twice that of a SSB receiver should also be indicated explicitly. For example: "When it comes to DSB radiometer, the ϵ need to be divided by sqrt(2) and \beta is twice that of the SSB. "

Reply: We are very sorry for our fault. We have checked that the noise equivalent bandwidth of a DSB receiver is the same as an SSB receiver. It is our misunderstanding in former answer. The sentence has been deleted.

As the Reviewer 3 comments: "I'm not sure about the sqrt(2). Surely it is only needed if the Tsys is defined in terms of single sideband for a double sideband receiver."

Tsys in Table 1 has been updated in terms of our latest design and a new simulation is performed. Tsys is 1000 K, 1000 K, 1000 K, 2300 K for 118 GHz, 190 GHz, 240 GHz, 643 GHz radiometers. This is a single-sideband value for 118 GHz radiometer, and double-sideband value for other radiometers. The corresponding noise is 2.2 K, 2.2 K, 2.2 K, 5.1 K.

This equation gives the noise STD expressed in the unit of "brightness temperature" (Rayleigh Jeans temperature) but the authors explained in their answer to my first review that they do not use this unit. They should clarify the unit issue here

Reply: Done. A sentence has been added:

"Planck function is used to compute the brightness temperature"

P12, Eq16: I think the equation is not used and should be removed.

Reply: Done.

P12L9-11: The following section is not clear: "The ideal rectangle channel response function is used. The simulation antenna patterns of the four radiometers are shown in Fig. 8. As the antenna calibration can be done by a linear function, it has no impact on the following simulation, so antenna pattern is not added in simulation below." Do the authors mean that they use an ideal rectangle channel function instead of the antenna patterns in Fig 8 ? If yes, they should rephrase it and

indicate the widths for all radiometer (one function per radiometer). I think that such an approximation is fine for the error estimations presented in this study, but it has to be clearly explained. Note that the scan vertical velocity should be taken into account. What does "antenna calibration" mean in "As the antenna calibration can be done by a linear function, it has no impact on the following simulation, ..."?

Reply: The ideal rectangle backend channel response function is used in the spectrometer simulation.

We are sorry there are some mistakes in the former simulation, a new simulation has been performed and the antenna patterns shown in Fig.8 are used. The section has been rephrased:

"The full-width at half-power points of antenna patterns are used in the following simulation"

P12L15: It is stated that "... the spectra are obtained every 2.5 km." but in Tab. 1 it is shown 1 km. What is the correct value?

Reply: We are sorry for this mistake. The spectra are obtained every 1 km. It has been corrected.

P12L15: Is "we use 2.5 km as the vertical resolution" for the retrieval layer? This statement is unclear. Is it the tangent height spacing or antenna FOV vertical resolution or the retrieval layer resolution?

Reply: It is the retrieval layer resolution. The sentence has been rephrased:

"A retrieval grid with 2.5 km spacing is used since it can match the FOV of TALIS well, and cutting down the size of the state vector will give a significant increase in speed (Livesey and Snyder, 2004)"

P12L7: "The retrieval grid resolution is 1 km below 25 km, 2.5 km below 50 km, and 5 km above 50 km." The choice of 1 km for retrieval layer below 25 km should be explained. In my point of view it is not an "optimal" choice for 2 reasons: 1) it is not consistent with the 2.5 km spacing of the tangent heights, and 2) only the 640 GHz radiometer can measure with a resolution better than 1 km.

Reply: Yes, that is right. We have realized the choice is not an "optimal" one. We have changed the retrieval grid resolution to 2.5 km in new simulation.

*P13L8: I still have trouble with the noise estimation. If I applied Eq 9 to the DBS receiver and taking into account that beta is 2 x spectrometer bandwidth I have: Noise STD at 640 GHz = 3.35 K (=3000/ sqrt(0.1*4.e6)/sqrt(2), with dt = 0.1 sec, beta=4.e6 Hz) This value is smaller than that given by the authors (5 K) by a factor close to sqrt(2). Also the radiometer should be indicated in the sentence: "... to be 2 K, 1.7 K, 1.7 K, and 5 K , respectively." -> "... to be 2 K, 1.7 K, 1.7 K, and 5 K at 118, 190, 240, 640 GHz, respectively."*

Reply: We are very sorry for misleading you. The fault explanation is discussed above. We have updated the Tsys and recalculated the noise in new simulation. The sentence has been rephrased:

"The expected 1σ noise is calculated by Eq. (9), the noise is assumed to be 2.2 K, 2.2 K, 2.2 K, and 5.1 K at 118, 190, 240,

643 GHz, respectively"

Fig9: The plots on the third panel are not visible. A log scale should be used.

Reply: Done.

P15L1: What is the error covariance matrix considered here: Sm (Eq 15) or Sm + Sn (Eq 15 and Eq 16)? In several figures (e.g., Fig 13), the retrieval error is larger than 100%. How it is possible if the a priori error is set at 100%

Reply: The error covariance matrix considered here is Sm + Sn (Eq 14 and Eq 15). A sentence has been added:

"The error covariance matrix used in following simulation is the total of $\boldsymbol{S}_n$ and $\boldsymbol{S}_m$."

We found the a priori error is set at 110%, it has been corrected in paper.

P15L10: The altitude range for good retrievals should be indicated (15-85 km).

Reply: Done.

P15L12: It is difficult to check the vertical resolution between 15 and 25 km, though the value of 2.5 km looks correct above 20 km. Below 20 km the resolution looks poorer.

Reply: Yes, the resolution is poorer below 20 km. The figures have been plotted again and a top x-axis is added in order to show the resolution clearly.

P15L13: "and TALIS is lack of the information." -> "where TALIS lacks sensitivity."

Reply: Done.

P15L15: The authors should provide values to support the statement. For example: "is better in in the upper troposphere (error of 2 K for a vertical resolution of 3-4 km between 10 and 15 km)"

Reply: Done. The sentence has been rephrased:

"However, the 240 GHz product can compensate for the loss of information since the precision is better in in the upper troposphere (error < 1 K for a vertical resolution of 2.5-3 km between 10 and 15 km)"

P17L7: It worth to indicate that O3 can be measure down to 10 km but with relatively low precision (50% and vertical resolution of 3-5 km).

Reply: Done. In new simulation, the precision at 10 km is also good. A sentence has been added:

"The profile can be retrieved with a single scan precision < 10% from 10 to 55 km and the vertical resolution is 2.5–3 km"

P21L4-8: I think the diurnal change of ClO should be discussed. The ClO profile corresponds to daytime and the nighttime relative precision will be worse between 30-40 km (ClO vanishes during nighttime). In the polar regions, the relative precision will be high between 20 and 25 km during chlorine activation.

Reply: Done. A sentence has been added:

"Since ClO will vanishes in the middle stratosphere (30-40 km) during nighttime, the precision will be worse in the nighttime. In the polar regions, the relative precision will be high between 20 and 25 km during chlorine activation"

Reviewer 3

We would like to sincerely thank the reviewer for his comments. We believe they help us to improve the manuscript significantly and give us many useful suggestions to improve the mission. We have corrected the manuscript according reviewer's comments and answer the reviewer's question point by point below.

Reviewer comments are in italic blue, the manuscript modifications are in red. The answer "Done" means that the manuscript has been modified following exactly the reviewer comment.

Reply to Specific comments

Page 1

Line 8/9: "high precision" means different things to different people (e.g., an airborne in situ instrument would most likely have way higher precision than anything remotely sounded). I'd simply changed it to something like "vertically resolved profile observations"

Reply: Done.

Line 11: The measurements clearly do not extend to the surface. I'd say "~10-100km, or "the upper troposphere to the mesosphere" or something like that.

Reply: Done.

Line 20: "or" -> "and/or"

Reply: Done.

Line 22: Delete "the"

Reply: Done.

Line 23: I suggest "...studies. Satellites can provide dailhy global coverage of the atmosphere. Instruments such as nadir microwave and infrared sounders have been applied..."

Reply: Done.

Page 2

Line 5, add a citation to Barath et al., 1993, doi:10.1029/93jd00798. Also to Waters et al., 1999, doi:10.1175/1520-0469(1999)056<0194:tuaeml>2.0.co;2

Reply: Done.

Page 3

Line 6: Please expand on the "higher" precision. It's not clear to me how the TALIS optical layout specifically enables that. Firstly, to be clear, you do mean "precision" (i.e., random noise-type errors) versus "accuracy" (more "systematic bias" type errors), correct? How does the optical layout improve that? Is it because there are fewer beam splitters etc. required? Also, please use terms like "better" and "worse" rather than "higher" and "lower" for terms like precision, accuracy and resolution. This is because when the words are used, having "more" sounds "better". However, when these terms are referred to quantitatively (e.g., with a noise level), then "more" sounds "worse".

Reply: Thank you for your correction. Yes, precision means random noise-type errors. We have corrected these terms in the paper.

The layout of TALIS can reduce the loss in the front end since there are fewer reflectors and mirrors. It will improve the sensitivity. The accuracy of calibration will also be improved since the targets can cover the four feeds.

Line 7: Please expand on the 20km displacement. Is this in azimuth (i.e., across the line-of-sight) or in elevetion (i.e., vertically) or some combination of the two? How does this modify your statement that the instrument scans from 0-100km, is it 0-100km for some receivers and 20-120 for others for example?

Reply: The 240 GHz radiometer has azimuth displacement. The 118 GHz and 190 GHz radiometer have elevation displacement.

For all radiometers, the scan range is 0-100 km, but there will be a sequence. For example, 118 Ghz will scan the surface firstly, then 643 GHz will scan it, 190 GHz is the last. All the data will be recorded as the 118 GHz start to work, so it has no impact on observation.

Line 10: Please expand on the calibration and instrument design overall. How do the antenna feeds in figure 2 "view the hot target"? Is the box at the end of the arm tipped up to look directly at the target? Does the target fold down to cover the feed horns?

Reply: The detail has been added to the caption of Figure 1.

"The reflector, feeds, and receivers are formed into a whole. The scan driver controls the scan angle. The calibration system is fixed in the satellite. At the beginning, the feeds are covered by calibration targets. Then it will scan the limb. When the system rotates to the top, it will view the cold space"

Figure 1: Please give more detail on the sketch or in the caption. Which parts of the instrument move to accomplish the scan? Is it just the antenna, just the feedhorn assembly, or both in concert. Alternatively, does the whole spacrcraft nod up and down?

Reply: Figure 1 has been changed. More details have been added. The scan driver will move with the whole (reflector, feeds, and receivers) to accomplish the scan.

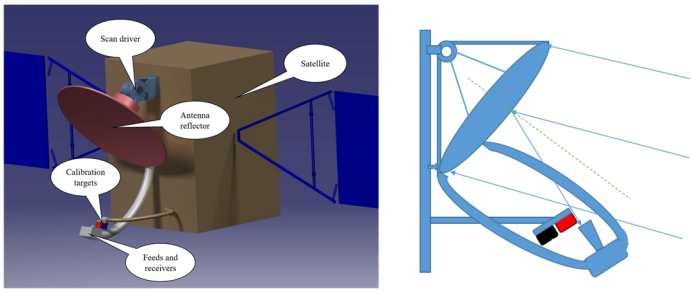

Table 1: Some of the numbers in the table (and in the discussion that follows) appear contradictory. If the instrument scans from 0-100km in 36 seconds, that's a rate of 2.7km per second. However, the integration time is quoted as "0.1s (1km)". Whatever the case, I've been assuming that all the distances quoted are "vertical", but some may think you're referring to the "along-track" distances (i.e., horizontal). It would be good to be clear on this.

Reply: TALIS spends 3 seconds to scan the hot target, 5 seconds to view the cold space, and 10 seconds to scan from 0-100 km. The total time of 36 seconds defined in paper includes scan and retrace (retrace also records data, it will spend 18 seconds), for one single scan it is 18 second. Yes, it is vertical distances, it has been corrected in paper.

Page 5

Line 6: It is not made clear to me (here or elsewhere) how the "broader bandwidth and finer resolution" is what leads to the improved performance over MLS. I grant that broad bandwidth counts in the lower parts of the atmosphere, but a lot of your improvements come in the mid-stratosphere where the lines are only a 10-100 MHz wide, so bandwidth is not an issue (unless you are bringing in additional lines, which works for ozone, which has many lines, but not water vapor). Are you

sure you're capturing the MLS characteristics correctly? As I understand it, the MLS 25-channel spectrometers cover their full bandwidth - as the channels become more widely separated away from the line centers, the channels also get wider increasing the signal to noise. There are no "gaps" in the spectral coverage, which is what the asterisks shown in Figure 3 seem to imply (it might be best to replace the asterisks in Figure 3 with horzontal lines of the correct channel-width, or something similar to make that point). Table 2 and Figure 7 of the Waters et al. 2006 reference shows the MLS configuration, please be sure you're capturing it correctly. I suggest you contact the MLS team if you are in any doubt (they are typically fairly responsive). Further, you may have omitted the MLS "Digital Autocorrelator Spectrometers" that I believe provide very fine spectral resolution in the line centers for some species. These contribute to improved performance for MLS in the upper altitudes.

Reply: Thank you for your suggestion. The MLS characteristics are obtained from the reference (Waters et al. 2006). Our simulation configuration follows the information shown in Table 4 and Figure 7 of the Waters et al. 2006. We believe the characteristics are set correctly. The channel-width has been added to Figure 3. In order to compare the performance of spectrometer, all other factors (includes noise) are set the same, only the bandwidth and resolution are different.

The improvements below 20 km mainly come from the bandwidth since the lines are wide. The improvements in the mid-stratosphere and above, the possible reason is the resolution. The 'DAS' spectrometers of MLS are not considered in the paper, it actually improves the performance in the mesosphere. The 25-channel spectrometer has relatively poor resolution.

A statement has been added:

"However, the Digital Autocorrelator Spectrometers of MLS which can improve the performance in the mesosphere are not considered here"

Pages 6-9, Figures 4-7.

It would be really helpful if the colors for each molecule could be consistent from band to band, at least for the main ones that are common to all many plots (O3, H2O, HNO3).

Reply: Done.

Page 9

Line 13: Poor wording: "Scattering can usually be negelected above the upper troposphere as the atmosphere is largely cloud-free at these altitudes, and such clouds as there are (e.g., Polar Stratospheric Clouds) have particle sizes shorter than the TALIS observation wavelengths.

Reply: Done. The sentence has been rephrased.

Page 10

Line 6: I don't think that's what the definition of "spectroscopy" is. How about "Spectroscopy models and databases allow us

to compute the absorption coefficient..."

Reply: Done. The sentence has been rephrased.

Line 15: Delete "needs" and change "convert" to "converts"

Reply: Done.

Line 16: Change to "... intermediate frequency, folding the upper and lower sideband signals together in consequence".

Reply: Done.

Page 11

Line 9: I'm not sure about the sqrt(2). Surely it is only needed if the Tsys is defined in terms of single sideband for a double sideband receiver.

Reply: We are sorry for this fault. The sentence has been deleted. Tsys in Table 1 has been updated in terms of our latest design and a new simulation is performed. Tsys is 1000 K, 1000 K, 1000 K, 2300 K for 118 GHz, 190 GHz, 240 GHz, 643 GHz radiometers. This is a single-sideband value for 118 GHz radiometer, and double-sideband value for other radiometers. The corresponding noise is 2.2 K, 2.2 K, 2.2 K, 5.1 K. The sentence has been rephrased:

"The expected 1σ noise is calculated by Eq. (9), the noise is assumed to be 2.2 K, 2.2 K, 2.2 K, and 5.1 K at 118, 190, 240, 643 GHz, respectively"

Line 30, Equation 14. Which of the covariance matrices are shown summarized as "Error" in the figures that follow? Looking at the plots I actually think it's the total of Eq 14 and Eq 15, but I'm not sure.

Reply: Yes, the error is the total of Eq 14 and Eq 15. A sentence has been added:

"The error covariance matrix used in following simulation is the total of $\boldsymbol{S}_n$ and $\boldsymbol{S}_m$"

Page 12

Line 10: I'm worried about the authors' choice to ignore the finite size of the field of view in the discussion that follows. It really is no additional hardship with ARTS to add that step, and would make for a far more meaningful study. If nothing else, I urge them to quantify the impact it has, which will not be on the precision so much as the vertical resolution.

Reply: We have added the antenna patterns shown in Fig.8 to our new simulation. The sentence has been rephrased:

"The full-width at half-power points of antenna patterns are used in the following simulation"

Line 14: Are they refering to the vertical resolution of the radiance obsevations or of the state vector vertical grid here? In either case, why is the FOV for TALIS or MLS germain to that choice? The tradeoff they are referring to with the Livesey

and Snyder paper is not really related to the resolution of the reporting grid, rather to the resolution of the information yield (e.g., as represented by the width of the averaging kernels). Also, if the spectra are obtained avery 2.5km what is the integration time assumed, and the total time taken for the vertical scan. Again, as with the numbers in Table 1, there is an inconsistency here. Fundamentally there are multiple "resolutions" at play here: The spacing of the retrieval grid, the spacing of the radiances, and the degree of information content in the Level 2 data products. Please try to be clear which you are referring to in each case.

Reply: We are sorry there are some mistakes in the former simulation, and have been corrected in new simulation. The spectra are obtained every 1 km, it is according to the numbers in Table 1. The spacing of the retrieval grid is 2.5 km in order to match the field of view. The sentence has been rephrased:

"A retrieval grid with 2.5 km spacing is used since it can match the FOV of TALIS well, and cutting down the size of the state vector will give a significant increase in speed (Livesey and Snyder, 2004)"

Paragraph starting at line 14, and through to end of 4.1: I think more information is needed in this section. Firstly, from where did the various atmospheric profiles assumed as "truth" and "apriori" come from? It just says "mid-latitude summer conditions". Are MLS data the source of the profiles? If so, please be explicit about the version of MLS data used, latitude/date range used, application of quality screening, assmptions made to go from pressure to altitude as the vertical coordiante etc. What about the species that MLS doesn't measure, ro doesn't measure well? If the profiles instead come from a model, again give all the information needed to suppor reproducibility. Secondly, in the retrieval calcaultions that follow, are the various molecules retrieved simultaneously from all the bands together, or are some subset (which) of the molecules retrieved independently from each band? Are there also spectrally flat (or simple linear or quadratic form) "Baseline" or "Extinction" terms included in the retrievals. These are needed to account for instrumental/forward model issues, and can impact the precision/resolution trade.

Reply: The profiles are provided by ARTS which is extracted from FASCOD. The BrO and HO_2 profiles are not included in ARTS-XML-DATA, so we use MLS L3 monthly averaged data (observed from 20°N-30°N in July, 2018). The molecules are retrieved simultaneously from each band. Spectrally flat is not included. The sentence has been rephrased:

"A mid-latitude summer atmospheric condition extracted from FASCOD which is provided by ARTS (profiles of BrO and HO2 are from MLS L3 monthly averaged data, 20°N-30°N, July, 2018) is chosen to perform the simulation"

"The molecules are retrieved simultaneously from each band"

Page 13

Line 3: Again, where does the "typical profile" come from

Reply: Answered above.

Line 4: In my experience the Gaussian form is a poor choice for the off-diagnoal terms, as it gives a normal equation matrix that is close to singularity. Instead an exponential form is generally preferred (and corresponds to a 1st-order Tikhanov smoothing).

Reply: Done, in our new simulation, the exponential form is used.

Line 10: How much averaging is the factor of 10 equivalent to? Presumably 100x as many measurements, correct? Please put that in terms a reader will readily understand (e.g., "equivalent to a 10-degree latitude weekly zonal mean" or whatever it is).

Reply: Done. A statement is added:

"equivalent to a 10-degree latitude weekly zonal mean"

Line 16: As stated above, I find it hard to believe the spectral resolution and bandwidth alone accounts for the MLS/TELIS differences shown, especially above ~20-30km. Are the authors sure they have correctly captured the MLS spectral coverage (see above)? The effective bandwidth (i.e., the width of the spectral regions that actually contain information) are essentially the same between the two instruments. Are the authors using the same system temperatures for both instruments (as strongly implied by line 16) or are they in fact changing those numbers too, if so that's the likely cause. Note the discussion of sqrt(2) above, I'm pretty sure the MLS team quotes thir system temperatures without invoking that factor. This is an important issue that warrants greater investigation.

Reply: Yes, the MLS spectral coverage is captured from (Waters et al. 2006). In simulation, only resolution and bandwidth of the two instruments are different, and the noise assumed are the same.

Figure 9 (and others): Please make it clear what "error" means in this context. Is it the sqrt-diagonal of one of the covariance matrices quoted above (or the sum of several)? Please be clear. I suggest the authors add some clear metric of vertical resolution to the right-hand figure (e.g., full width at half maximum, or degrees of freedom per km), with a separate top x-axis.

Reply: The error covariance matrix has been stated:

"The error covariance matrix used in following simulation is the total of $\boldsymbol{S}_n$ and $\boldsymbol{S}_m$"

Done. The figures have been plotted with the top x-axis to show the FWHM.

Page 15

Line 1: Again, which covariance matrix!

Reply: Answered above.

Figure 12 and its siblings: I really don't see the point of showing a single retrieved noisy profile here, it's but one representative retrieval exhibiting noise and risks giving the uneducated reader the impression of some kind of systematic biases that cannot be reduced. Related to that, is the "Error" term again the sqrt of some covariance diagonal, or is it the difference between retrieved and true (I don't think so, looking at the results, but some readers may get confused). I'd just simply show the retrieved precision, and the typical profile (combining the first two panels into one with only two lines).

Reply: Done.

Page 16

Line 8: "less" -> "poorer"

Reply: Done.

Page 24

Line 5: As discussed, it's essentially impossible for the reader to "see" the 3km resolution from your figures. Please add some suitable line/plot to make that clerer.

Reply: Done.

Line 10: "Significantly average" -> "Significant averaging"

Reply: Done.

Page 29

Line 5: Change first sentence to: "Seven species show high sensitivity, sufficient for scientifically useful single profile retrievals".

Reply: Done.

Line 23/24: Just a note, the Zeeman effect will indeed be critical to the correct retrieval of mesospheric temperature, though it will probably not impact the precision/resolution results shown here.

Reply: Thank you for your note, we will add Zeeman effect in future study.

Performance Evaluation of THz Atmospheric Limb Sounder (TALIS) of China

Wenyu Wang[1,2], Zhenzhan Wang[1], Yongqiang Duan[1,2]

[1]Key Laboratory of Microwave Remote Sensing, National Space Science Center, Chinese Academy of Sciences, Beijing, China
[2]University of Chinese Academy of Sciences, Beijing, China

Correspondence to: Zhenzhan Wang (wangzhenzhan@mirslab.cn)

Abstract. THz Atmospheric Limb Sounder (TALIS) is a microwave limb sounder being developed for atmospheric ~~high precision observation~~ vertically resolved profile observations by the National Space Science Center, Chinese Academy of Sciences (NSSC, CAS). It is designed to measure the temperature and chemical species such as O_3, HCl, ClO, N_2O, NO, NO_2, HOCl, H_2O, HNO_3, HCN, CO, SO_2, BrO, HO_2, H_2CO, CH_3Cl, CH_3OH, and CH_3CN with high vertical resolution from ~~surface to about~~ about 10-100 km to improve our comprehension of atmospheric chemistry and dynamics, and to monitor the man-made pollution in the atmosphere. Four heterodyne radiometers including several FFT spectrometers of 2 GHz bandwidth with 2 MHz resolution are employed to obtain the atmospheric thermal emission in broad spectral regions centred near 118, 190, 240, and 643 GHz. A theoretical simulation is performed to estimate the retrieval precision of the main targets and to compare them with that of MLS standard spectrometers. Single scan measurement and averaged measurement are considered in simulation, respectively. Temperature profile can be obtained with the precision of < 2K for a single scan from ~~15~~10 to ~~85~~60 km by using 118 GHz radiometer, and the 240 and 643 GHz radiometer can provide temperature information in the upper troposphere. Chemical species such as H_2O, O_3, HCl show relatively high single scan retrieval precision of ~~1~~ ≤ 20% over most of the useful range and ClO, N_2O, HNO_3 can be retrieved with a precision < 50%. The other species should be retrieved by using averaged measurements because of the weak intensity and/or low abundance.

1 Introduction

~~High~~ Better precision observation of ~~the~~ Earth's atmosphere is essential to the numerical weather prediction and climate change studies. ~~The satellite can provide global coverage atmospheric monitoring in a short time~~ Satellites can provide daily global coverage of the atmosphere. Instruments such as nadir microwave sounder and infrared sounder have been applied to measure the atmospheric temperature and humidity but with the poor vertical resolution and altitude range (Swadley et al., 2008). Limb sounders can not only provide the temperature profile with better vertical resolution but gather information on chemical composition in a wide altitude range. In the terahertz domain, the measurement performances are independent of the day-night cycle. Microwave limb sounding is a particularly useful technique in detecting stratospheric

and mesospheric temperature and chemistry, and also has large potential for global wind measurement in the middle and upper atmosphere (Wu et al., 2008; Baron et al., 2013).

A few instruments have been launched in recent twenty years, their observation data have offered a better understanding of the physical and chemical processes in the Earth's atmosphere. The first instrument applying the microwave limb sounding technique from space was the Microwave Limb Sounder (MLS) onboard the Upper Atmosphere Research Satellite (UARS) launched in 1991. The sounder offered unique information of temperature/pressure, O_3, H_2O, ClO, and additional data products including SO_2, HNO_3, and CH_3CN (Waters et al., 1993; Barath et al., 1993; Waters et al., 1999). The Sub-Millimetre Radiometer (SMR) onboard the Odin satellite launched in February 2001 was the first radiometer to employ sub-millimetre in limb sounding. Various target species such as O_3, ClO, N_2O, HNO_3, H_2O, CO, NO, as well as isotopes of H_2O, O_3, and ice cloud have been detected (Murtagh et al., 2002; Urban et al., 2005; Eriksson et al., 2007). Aura MLS, the follow-on of UARS MLS onboard the Aura satellite launched in July 2004 gave successful observations of OH, HO_2, H_2O, O_3, HCl, ClO, HOCl, BrO, HNO_3, N_2O, CO, HCN, CH_3CN, SO_2, ice cloud, and wind (Waters et al., 2004; Waters et al., 2006; Wu et al., 2008; Livesey et al., 2013). The Superconducting Submillimeter-wave Limb-Emission Sounder (SMILES) onboard the Japanese Experiment Module (JEM) of the International Space Station (ISS) launched in September 2009 (Kikuchi et al., 2010). SMILES was equipped with 4K cooled Superconductor–Insulator–Superconductor (SIS) mixers to reduce the system noise temperature so that the sensitivity of the SMILES was higher than that of other similar sensors such as MLS and SMR (Takahashi et al., 2010; Baron et al., 2011). Currently, several new instruments are being developed. Stratospheric Inferred Winds (SIW) is a Swedish mini sub-millimetre limb sounder for measuring wind, temperature, and molecules in the stratosphere. It can provide horizontal wind vectors within 30–90 km, as well as the profiles of temperature, O_3, H_2O and other ~~abundant~~ trace chemical species (Baron et al., 2018). SIW is designed for small satellites and will be launched as early as 2020–2022. In addition, the follow-on of SMILES, SMILES-2, is being studied for measuring the whole vertical range of 15−180 km with low noise (Ochiai et al., 2017).

THz Atmospheric Limb Sounder (TALIS) is the pre-research project of civil aerospace technology proposed by China National Space Administration (CNSA). TALIS is being designed at National Space Science Center, the Chinese Academy of Sciences (NSSC, CAS) for ~~high~~ good precision measurement of atmospheric temperature and key chemical species. It has four microwave radiometers in the frequency bands of 118, 190, 240, and 643 GHz which are similar to Aura MLS. TALIS mission objectives are to provide the information for research on the dynamics and the chemistry of the middle and upper atmosphere by measuring the volume mixing ratio (VMR) profile of the chemical species and other atmospheric condition such as cirrus with much finer spectral resolution. The pre-research will be completed in 2020 and a prototype will be tested. The satellite mission equipped with TALIS will be proposed around 2021.

In this paper, we present a simulation study on precision estimates for the geophysical parameters measured by TALIS. The outline of the present study is as follows: Section 2 describes the instrument characteristics and spectral bands. The

retrieval method and the simulation result are discussed in Sects. 3 and 4, respectively. The final section gives a conclusion about the performance and future works.

2 Instrument overview

2.1 Instrument characteristics

The TALIS payload (Fig. 1) and its proposed scan characteristics are summarized in Table 1. The instrument will be set at a sun-synchronous orbit at a normal altitude of 600 km. The offset parabolic antenna is made of a single reflector with 1.6 m projective aperture and four independent feeds. The layout of four discrete feeds is shown in Fig. 2. Compared with the quasi-optical separation layout (such as MLS), this strategy is easier and has ~~higher~~ better observation precision since it needs fewer reflectors. But it will lead to a vertical observed difference of about 20 km between ~~the four radiometers~~118, 190, and 643 GHz and horizontal displacement of 240 GHz. The widths of the field of view (FOV) at the tangent point are about 5.5, 3.8, 3.3, and 0.96 km at 118, 190, 240, 643 GHz, respectively. The two-point calibration method is adopted by TALIS, and ~~an extra~~two calibration targets ~~is~~ are set at the ~~bottom of the antenna~~ end of the arm. The extra target can be used to improve the calibration precision and evaluate the antenna effect and nonlinearity. At the beginning of the scan, TALIS will view the hot target (ambient temperature) and the extra target (lower temperature) in 3 s, and then it will scan the limb from 0 to 100 km vertically and obtain the spectra every 1 km with an integration time of 0.1 s, finally, it views the cold space at 200 km in 5 s. The process of retrace is the same (also record data) and giving a total period (scan and retrace) of about 36 s.

TALIS has four radiometers which cover the significant thermal emission spectra in the 118, 190, 240, and 643 GHz regions (see Table 2). Single-sideband (SSB) can keep the complete spectral lines while double-sideband (DSB) can cover more spectral lines because of the image band. Thus, all the radiometers of TALIS will operate in the double-sideband mode except the 118 GHz radiometer. Eleven FFT spectrometers of 2 GHz bandwidth with 2 MHz resolution will be used in TALIS. The bands and system noise temperature for each radiometer are shown in Table 2.

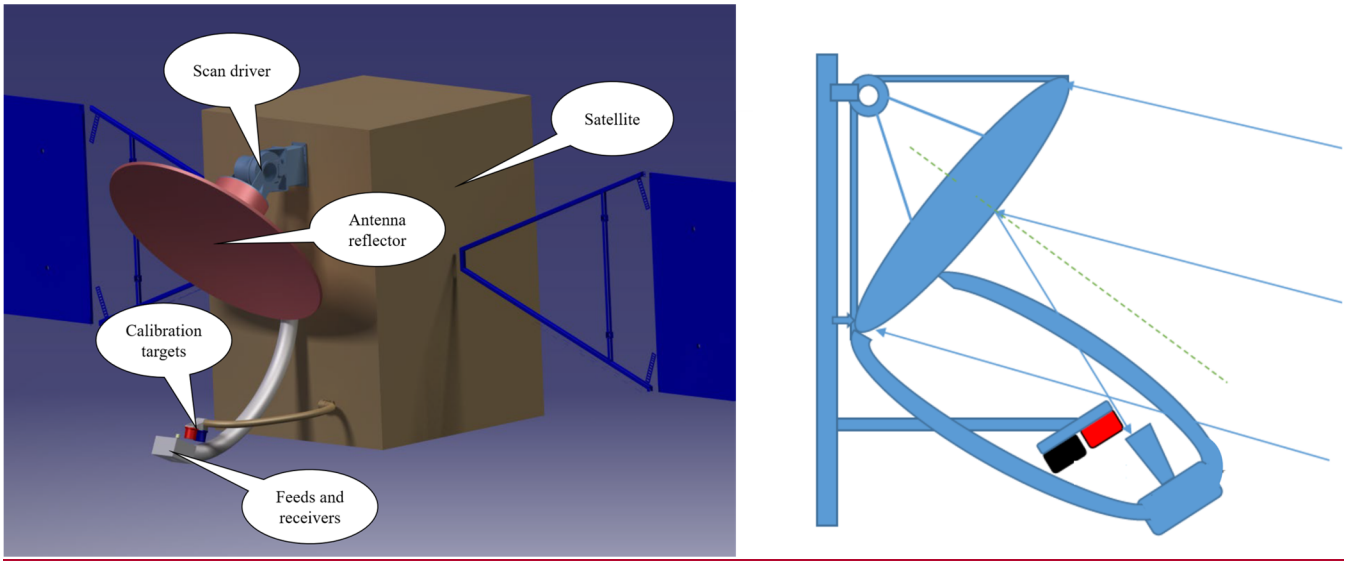

Figure 1. The schematic diagram of TALIS payload. The reflector, feeds, and receivers are formed into a whole. The scan driver controls the scan angle. The calibration system is fixed in the satellite. At the beginning, the feeds are covered by calibration targets. Then it will scan the limb. When the system rotates to the top, it will view the cold space.

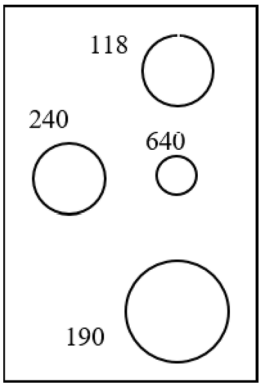

Figure 2. The layout of the four antenna feeds. There exists a vertical observed difference of about 20 km between 118, 190, and 643 GHz and horizontal displacement between 240 GHz and other three radiometers.

Table 1. Characteristics of the TALIS payload

Satellite altitude	600 km
~~Scan~~Vertical scan-altitude	0–100 km
LOS nadir angle	66.07–68.17°（2.1°）
Scan velocity	0.21°s^{-1} (36 s $scan^{-1}$)
Spectrum integration time	0.1 s (1 km)
Antenna size	1.6 m
Antenna vertical FOV	5.5, 3.8, 3.3, 0.96 km
Spectrometer Bandwidth	2 GHz
Spectrometer resolution	2 MHz

LO frequency	120, 190.1, 239.66, 642.87 GHz

Table 2. Spectral bands and Tsys of TALIS

Radiometer	TALIS (GHz)	Tsys* for TALIS	Tsys for MLS	Radiometer	TALIS (GHz)	Tsys for TALIS	Tsys for MLS
118 GHz	117.75–119.75	~~800~~ 1000 K	1200 K	240 GHz	229.66–231.66 247.66–249.66	1000 K	1200–1600 K
190 GHz	175.5–177.5 202.7–204.7	1000 K	900–1100 K		232.16–234.16 245.16–247.16		
	178.9–180.9 199.3–201.3				234.66–236.66 242.66–244.66		
	183.0–185.0 195.2–197.2			643 GHz	624.47–626.47 659.27–661.27	~~3000~~ 2300 K	4000–4400 K
					627.37–629.37 656.37–658.37		
					632.37–634.37 651.37–653.37		
					634.87–636.87 648.87–650.87		

* This is a single-sideband value for 118 GHz radiometer, and double-sideband value for other radiometers.

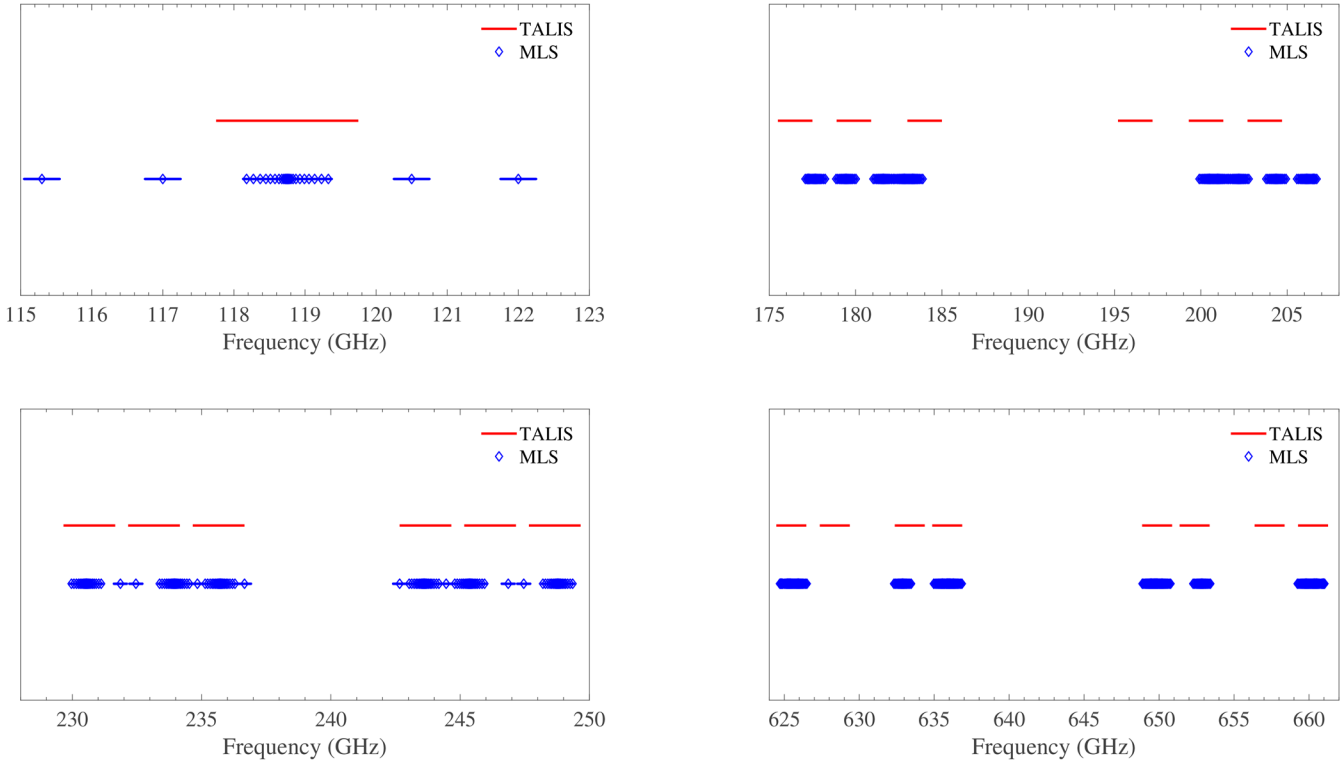

Figure 3. Spectral bands of Aura MLS and TALIS radiometers. **The diamond represents the line centers, and the solidline means the bandwidth of MLS.**

2.2 Spectral bands

The spectral bands of TALIS are selected with the following criteria: (1) maximizing the number of species which will exert a strong influence on atmospheric chemistry and dynamics, (2) necessary space between the passband, (3) trade-off between realizable bandwidth and resolution. TALIS covers most spectral bands of Aura MLS and extends them (see Fig 3), but lack the 2.4 THz band. The broader bandwidth and the finer resolution of TALIS can provide ~~higher~~ better retrieval precision and effective altitude range compared with Aura MLS. More chemical species can be measured by TALIS, such as NO_2, NO, and SO_2 (normal concentration).

The 118 GHz radiometer, covering the strong O_2 line at 118.75 GHz, is used to measure the atmospheric temperature and tangent pressure. Since there are few meteorological data set about the temperature above the middle atmosphere with good vertical resolution, it is necessary to measure the temperature profile with wide altitude range, good vertical resolution, and ~~high~~ good precision. In addition, the Zeeman effect will affect the O_2 line, the influence should be studied (Schwartz et al, 2006). Other information such as ice cloud can be treated as additional measurement. Figure 4 gives an overview of the 118 GHz spectral band.

The 190 GHz radiometer is mainly designed to cover the 183.31 GHz H_2O line. Monitoring water vapour is important for understanding the mechanisms that humidity feedback on climate, and is essential for improving the accuracy of the weather forecast. Other chemical species such as N_2O, ClO, O_3, and HCN are also included in 190 GHz bands (see Fig. 5).

The main objective of the 240 GHz radiometer is to measure the CO at 230.54 GHz and the strong O_3 lines in a wide spectral band where upper tropospheric O_3 can be obtained with ~~high~~ good precision because of the weak water vapour continuum absorption. In addition, the 233.95 GHz O_2 line will be used to measure temperature and tangent pressure together with 118.75 GHz line. SO_2 is an important pollutant in the Earth' atmosphere and will give rise to acid rain. There is no obvious SO_2 emission with the standard profile present in the passband of 240 GHz radiometer. The only SO_2 which is observable by

MLS comes from volcanic eruptions. MLS demonstrated that SO_2 can be measured by 190 GHz, 240GHz, and 640 GHz radiometer, but only 240 GHz SO_2 product is recommended for general use (Pumphrey et al., 2015). The wide and strong lines of HNO_3 can be used to retrieve profile well. NO_2 is a unique species not covered by Aura MLS, and TALIS's wider bandwidth and finer resolution have the potential ability to measure it. The spectra of 240 GHz radiometer are depicted in Fig. 6.

The 643 GHz radiometer is designed to cover as many spectral lines as possible, thus about 17 species are included. The spectral lines covering O_3, HCl, ClO, N_2O, O_2, and H_2O are clearly visible (Fig. 7), and other lines which are relatively weak such as NO, HNO_3, CO, SO_2, BrO, HO_2, H_2CO, HOCl, and CH_3Cl, can also be used. The O_2 line at 627.75 GHz and the H_2O line at 657.9 GHz have the potential to be used as supplements to 118 and 190 GHz radiometers. O_3 is the major species in the stratosphere and mesosphere, which is quite important in atmospheric radiation transfer. Using the high sensitivity lines in the 643 GHz bands, one can measure O_3 with ~~high~~ good precision (Takahashi et al., 2011; Kasai et al., 2013). The

only lines of HCl below 1 THz are in the 625 GHz frequency band, thus HCl can be measured by 643 GHz radiometer (Lary and Aulov, 2008). ClO is a key catalyst for ozone loss and the 649.45 GHz line is suitable for ClO observation with good precision (Santee et al., 2008; Sato et al., 2012). The HOCl, which will affect stratospheric chlorine budget, has distinct lines above 600 GHz, and the 635.87 GHz line has been pointed out to be the best line for observation (Urban, 2003). Both 649.701 and 660.486 GHz lines can be used to measure the hydroperoxyl radical HO_2, which will contribute to the catalytic ozone chemistry in the upper stratosphere and mesosphere (Millán et al., 2015). Since ClO, HO_2, and HOCl all can be measured, the reaction rate of ClO and HO_2 to form HOCl in the atmosphere can be determined (Johnson et al., 1995). N_2O can be measured at 652.834 GHz, which has been validated by MLS (Lambert et al., 2007). NO has two weak signals at 651.45 and 651.75 GHz which can be used to measure the abundance. HNO_3 can be measured using 650 GHz bands. Measuring these nitrogen species will help researchers to understand the chemistry and dynamics of the atmosphere better. The BrO, which plays an important role in the depletion of ozone, can be measured using 624.768 and 650.179 GHz lines. Because of the low abundance of BrO, measurements must be significantly averaged in order to get reliable results (Millán et al., 2012). CO and H_2CO are the major species in the CH_4 oxidation to CO_2 and H_2O in the stratosphere and mesosphere (Suzuki et al., 2015). The major spectral line of CO used by MLS is at 230.538 GHz, however, the 661.07 GHz line can also provide information (Livesey et al., 2008). H_2CO has a line at 656.45 GHz, but the signal is very weak. The SO_2 lines in the 660 GHz band have the potential to detect the background levels of SO_2. CH_3Cl can be measured in the 649 GHz band near the line of ClO. MLS measured CH_3OH and CH_3CN in the troposphere and lower stratosphere by 625 GHz spectrometer (Pumphrey et al., 2011).

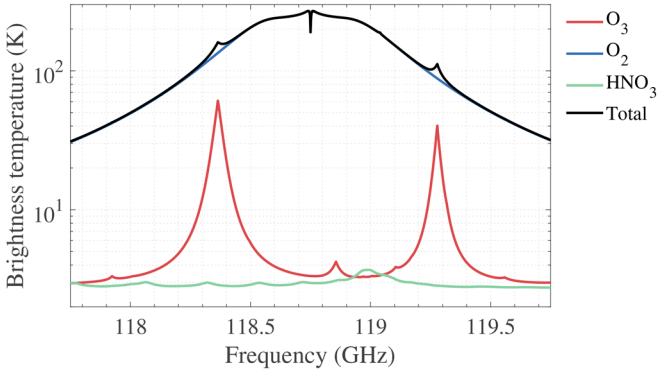

Figure 4. Contributions of the main target chemical species to the 118 GHz spectrum. The brightness temperature is measured from single sideband radiometer. The tangent height is 30 km.

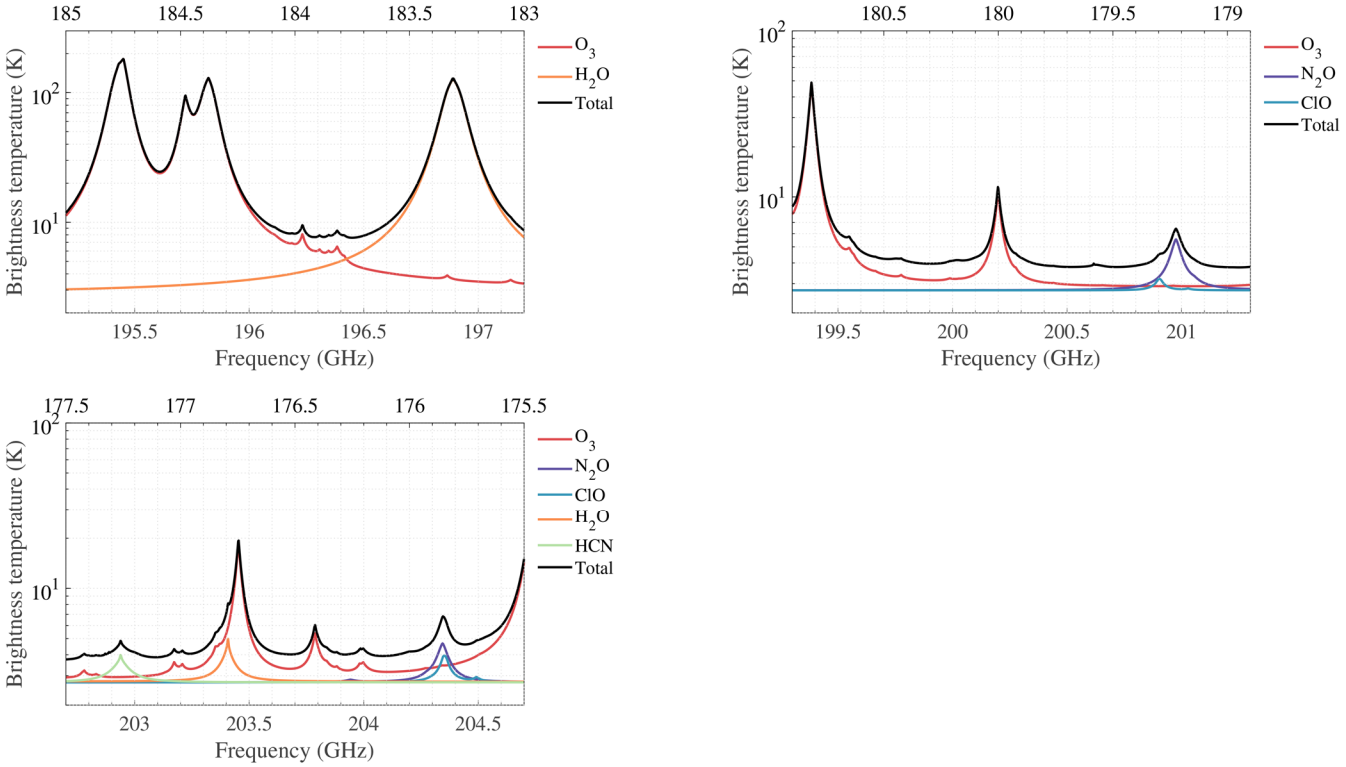

Figure 5. Contributions of the main target chemical species to the 190 GHz spectra. The brightness temperature is measured from double sideband radiometer. The tangent height is 30 km. The top axis represents the lower sideband frequencies and the bottom axis represents the upper sideband frequencies. Each panel represents a single spectrometer.

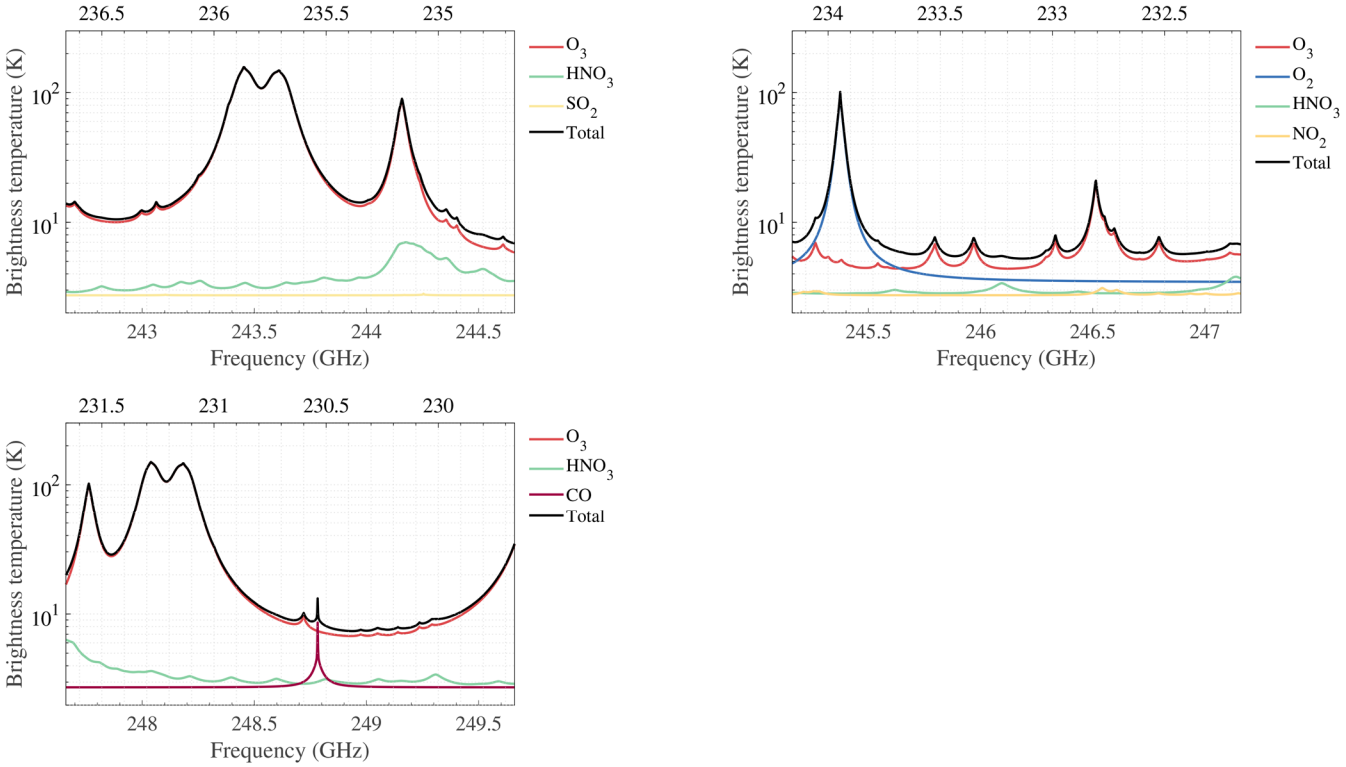

Figure 6. Contributions of the main target chemical species to the 240 GHz spectra. The brightness temperature is measured from double sideband radiometer. The tangent height is 30 km. The top axis represents the lower sideband frequencies and the bottom axis represents the upper sideband frequencies. Each panel represents a single spectrometer.

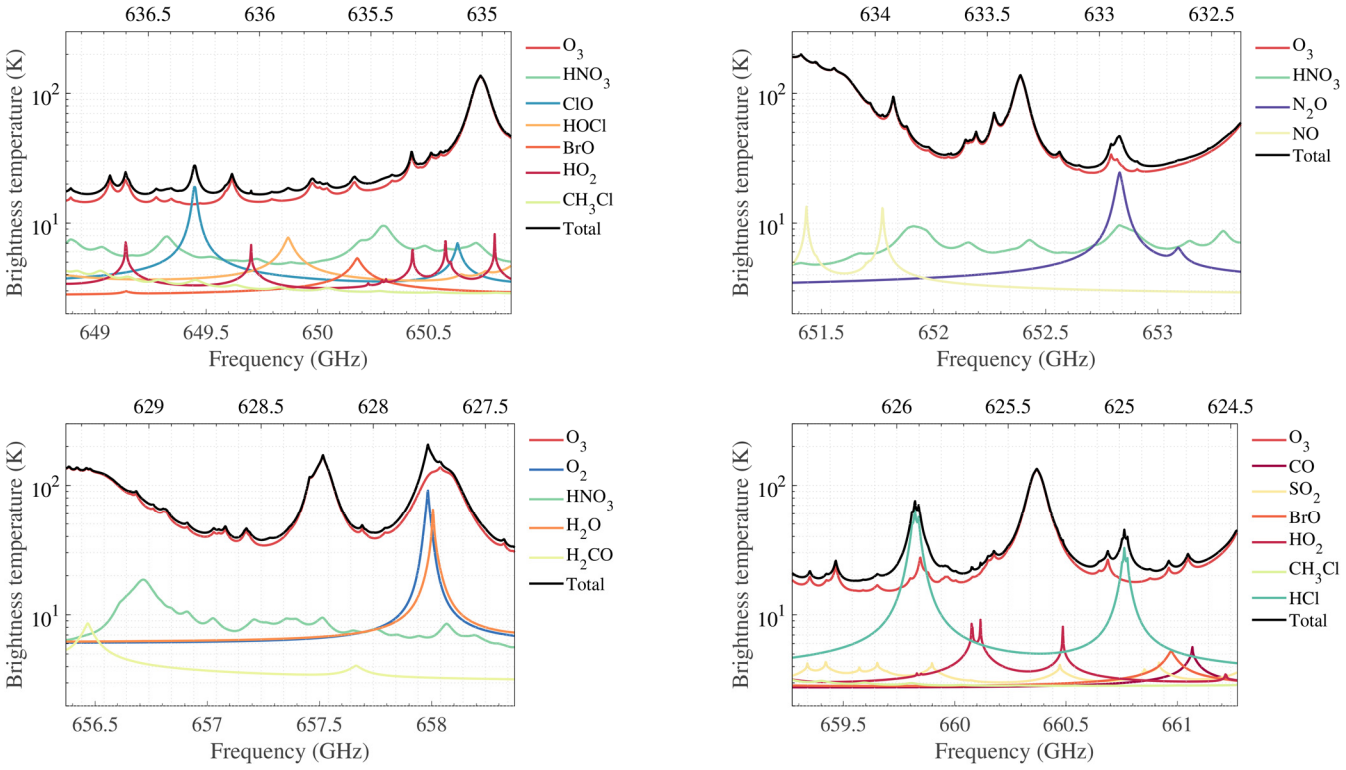

Figure 7. Contributions of the main target chemical species to the 643 GHz spectra. The brightness temperature is measured from double sideband radiometer. The tangent height is 30 km. The top axis represents the lower sideband frequencies and the bottom axis represents the upper sideband frequencies. Each panel represents a single spectrometer.

3 Retrieval methodology

3.1 Forward model

The retrieval of data measured by microwave limb sounder requires the accurate simulation of the observed thermal emission spectra. The forward model is a mathematical tool used to describe the radiative transfer, spectroscopy, and instrumental characteristics. The output of the forward model is the convolution of atmospheric radiation and instrument response.

Radiative transfer describes the emission, propagation, scattering, and absorption of electromagnetic radiation (Mätzler., 2006). ~~Scattering usually can be neglected above the upper troposphere because of the cloud free.~~ Scattering can usually be neglected above the upper troposphere as the atmosphere is largely cloud-free at these altitudes, and such clouds as there are (e.g., Polar Stratospheric Clouds) have particle sizes shorter than the TALIS observation wavelengths. In this way and assuming Local Thermodynamic Equilibrium (LTE), the formal solution of the radiative transfer equation is defined by

$$I_v(S_2) = I_v(S_1)e^{-\tau_{v(S_1,S_2)}} + \int_{S_1}^{S_2} \alpha_v(s)B_v(T)e^{-\tau_{v(S,S_2)}}ds, \quad (1)$$

where I_v is the radiance at frequency v reaching the sensor, α is the absorption coefficient and τ is the opacity or optical thickness. B_v stands for the atmospheric emission which is given by Planck function describing the radiation of a black-body at temperature T and frequency v per unit solid angle, unit frequency interval and unit emitting surface (Urban et al., 2004):

$$B_v(T) = \frac{2hv^3}{c^2}\frac{1}{e^{hv/k_BT}-1}, \quad (2)$$

where h is the Planck constant, c is the speed of light, k_B denotes Boltzmann constant.

~~Spectroscopy is the method to calculate~~ Spectroscopy models and databases allow us to compute the absorption coefficient which requires pressure, temperature, and the species concentrations along the line of sight. The basic expression can be written as:

$$\alpha(v) = nS(T)F(v), \quad (3)$$

where S is called the line strength, F means the line shape function, and n is the number density of the absorber.

Sensor characteristics also have to be taken into account by the forward model, including the antenna field-of-view, the sideband folding, and the spectrometer channel response (Eriksson et al., 2006).

Firstly, the radiance which encounters the antenna response could be expressed by the integration:

$$I_v^a = \int_\Omega I_v(\Omega)W_v^a(\Omega)d\Omega, \quad (4)$$

where W_v^a is the normalized antenna response function. Normally, the variation of I_v in azimuth angle dimension can be neglected or calculated before-hand. Secondly, a heterodyne mixer ~~needs to~~ converts the signals to intermediate frequency, ~~which will lead to a consequence that the lower and upper sideband are folded~~ folding the upper and lower sideband signals together in consequence. The apparent intensity after the mixer can be modelled as:

$$I_v^{if} = \frac{W_v^s(v)I_v^a + W_v^s(v')I_{v'}^a}{W_v^s(v) + W_v^s(v')}, \quad (5)$$

where W_v^s means the sideband response. At last, the final signal will be recorded by spectrometers, which can be described in a similar way as the antenna response:

$$I^c = \int_v I_v^{if} W_v^c(v)dv. \quad (6)$$

Here W_v^c means the normalized channel response, and the radiance is denoted I^c.

The measured radiance is transformed to brightness temperatures using the Planck's function.

3.2 Retrieval algorithm

Optimal estimation method (OEM) is the most common method used in atmospheric sounding for retrieving vertical profiles of chemistry species (Rodgers, 2000).

In OEM theory, a predicted noisy measurement $\hat{\boldsymbol{y}}$ can be expressed by a forward model $\boldsymbol{F}$ with an unknow atmospheric state $\boldsymbol{x}$ and the system noise ϵ_y according to:

$$\hat{\boldsymbol{y}} = \boldsymbol{F}(\boldsymbol{x}, \boldsymbol{b}) + \epsilon_y. \quad (7)$$

The noiseless predicted radiance $F(x, b)$ are compared with the observed radiance y so that the unknow state which minimize the cost function χ^2 could be found. The cost function is given by:

$$\chi^2 = [\boldsymbol{y} - \boldsymbol{F}(\boldsymbol{x}, \boldsymbol{b})]^T \boldsymbol{S}_y^{-1} [\boldsymbol{y} - \boldsymbol{F}(\boldsymbol{x}, \boldsymbol{b})] + [\boldsymbol{x} - \boldsymbol{x}_a]^T \boldsymbol{S}_a^{-1} [\boldsymbol{x} - \boldsymbol{x}_a], \quad (8)$$

where x_a is a priori state vector, $\boldsymbol{S}_a$ and $\boldsymbol{S}_y$ stand for the covariance matrices representing the natural variability of the state vector and the measurement error vector, respectively. Assuming there is no correlation between channels, the off-diagonal elements of $\boldsymbol{S}_y$ are zero and the diagonal elements are set to the square of the system noise. Usually, a simple formula can be used to determine the SSB radiometric noise standard deviation:

$$\epsilon = \frac{T_{sys}}{\sqrt{\beta\, d\tau}}, \quad (9)$$

where T_{sys} is the system noise temperature which is the sum of receiver noise temperature and the atmospheric temperature received by the antenna, β is the noise equivalent bandwidth and $d\tau$ is the integration time for measuring a single spectrum. ~~When it comes to DSB radiometer, the ϵ need to be divided by $\sqrt{2}$.~~ The diagonal elements of the S_a specify a priori variance and the off-diagonal terms are used to describe correlations between adjacent elements in order to make the retrieved profile smoother. Planck function is used to compute the brightness temperature.

Finally, the Levenberg–Marquardt method which is the modification of the Gauss-Newton iterative is used to solve the nonlinear problem. The solution is given by

$$\boldsymbol{x}_{i+1} = \boldsymbol{x}_i + \left[(\boldsymbol{I} + \gamma)\boldsymbol{S}_a^{-1} + \boldsymbol{K}_{xi}^T \boldsymbol{S}_y^{-1} \boldsymbol{K}_i\right]^{-1} \left\{\boldsymbol{K}_{xi}^T \boldsymbol{S}_y^{-1} [\boldsymbol{y} - \boldsymbol{F}(\boldsymbol{x}_i)] - \boldsymbol{S}_a^{-1} (\boldsymbol{x}_i - \boldsymbol{x}_a)\right\}, \quad (10)$$

where γ denotes the Levenberg–Marquardt parameter, and $\boldsymbol{K}_{xi}$ represents the weighting function matrix (Jacobian).

The OEM method provides an approach to describe the retrieval error completely. The averaging kernel matrix $\boldsymbol{A}$, which represent the sensitivity of the retrieved state to the true state, is written as:

$$\boldsymbol{A} = \boldsymbol{G}_y \boldsymbol{K}_x = \frac{\partial \hat{\boldsymbol{x}}}{\partial \boldsymbol{x}}, \quad (11)$$

where the G_y is the contribution matrix, which express the sensitivity of the retrieved state to the measurement:

$$\boldsymbol{G}_y = \frac{\partial \hat{\boldsymbol{x}}}{\partial \boldsymbol{y}} = \left(\boldsymbol{K}_x^T \boldsymbol{S}_y \boldsymbol{K}_x + \boldsymbol{S}_a^{-1}\right)^{-1} \boldsymbol{K}_x^T \boldsymbol{S}_y^{-1}. \quad (12)$$

The retrieval resolution can be estimated from the full width at half-maximum (FWHM) of the averaging kernel (Marks and Rodgers, 1993).

There is another useful variable defined as measurement response, which represents the true state contribution in the retrieval (Baron et al., 2002):

$$W(i) = \sum_j |A(i, j)|. \quad (13)$$

The ideal measurement response should be near 1. In practice, reliable range of a retrieval is usually characterised by $|W - 1| < 0.2$.

The ~~total~~ retrieval error can be described by ~~three~~ two covariance matrices, the smoothing error covariance matrix which is from the need of a priori information:

$$\boldsymbol{S}_n = (\boldsymbol{A} - \boldsymbol{I})\boldsymbol{S}_a(\boldsymbol{A} - \boldsymbol{I})^T, \quad (14)$$

the measurement error covariance matrix due to the measurement noise:

$$\boldsymbol{S}_m = \boldsymbol{G}_y\boldsymbol{S}_y{\boldsymbol{G}_y}^T, \quad (15)$$

The error covariance matrix used in following simulation is the total of $\boldsymbol{S}_n$ and $\boldsymbol{S}_m$.

~~and the model parameter error covariance matrix introduced by the uncertainties in the forward model:~~

~~$$\boldsymbol{S}_s = \boldsymbol{G}_y\boldsymbol{K}_b\boldsymbol{S}_b\boldsymbol{G}_y\boldsymbol{K}_b{}^T. \quad (16)$$~~

4 Measurement performance

4.1 Simulation setup

The objective of the simulation is to evaluate the observation performance of TALIS. In this simulation, the forward model Atmospheric Radiative Transfer Simulator (ARTS 2.3) and its corresponding retrieval tool Qpack2 are used (Eriksson et al., 2005; Eriksson et al., 2011). The instrumental setup follows the characteristics of TALIS described in Table 1 and Table 2. The ideal rectangle backend channel response function is used. The simulation antenna patterns of the four radiometers are shown in Fig. 8. ~~As the antenna calibration can be done by a linear function, it has no impact on the following simulation, so antenna pattern is not added in simulation below.~~The full-width at half-power points of antenna patterns are used in the following simulation.

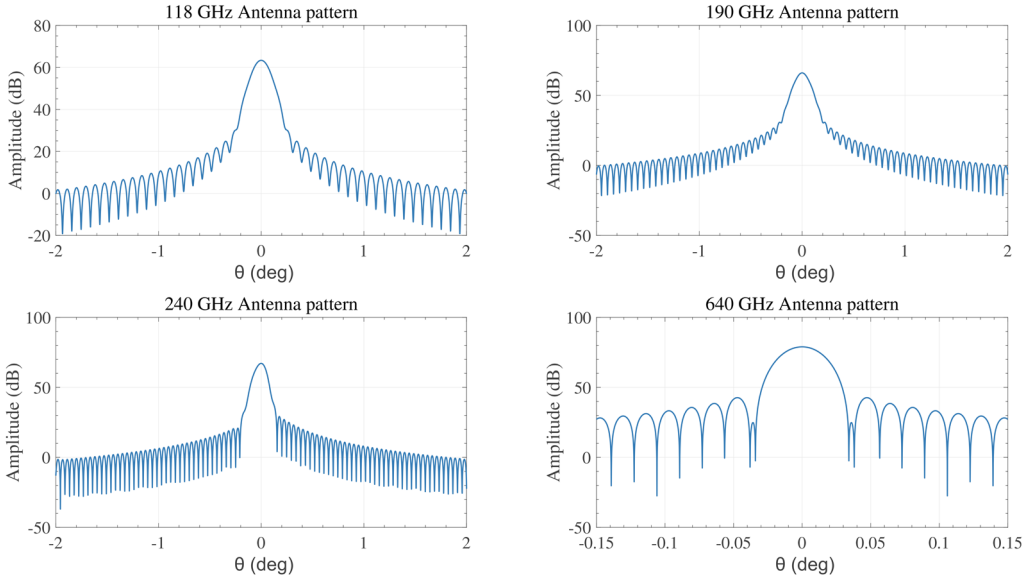

Figure 8. The antenna patterns of TALIS.

~~In this simulation, the scan altitude range is from 10 to 95 km and the spectra are obtained every 2.5 km. As the effective FOV of TALIS are similar to MLS, we use 2.5 km as the vertical resolution. It is the trade-off between the step of efficient limb observation and the optimum information can be obtained (Livesey and Snyder, 2004).~~

In this simulation, the scan altitude range is from 10 to 90 km and the spectra are obtained every 1 km. A retrieval grid with 2.5 km spacing is used since it can match the FOV of TALIS well, and cutting down the size of the state vector will give a significant increase in speed (Livesey and Snyder, 2004). A mid-latitude summer atmospheric condition extracted from FASCOD which is provided by ARTS (profiles of BrO and HO_2 are from MLS L3 monthly averaged data, 20°N-30°N, July, 2018) is chosen to perform the simulation. The scattering from tropospheric clouds, refraction, and Zeeman effect are not considered because of the large computational complexity. A spectroscopic line parameters catalogue created with the data taken from JPL catalogue (Pickett et al., 1998), HITRAN database (Rothman et al., 2013), and Perrin catalogue (Perrin et al., 2005) is used for line-by-line absorption calculation. The measurement covariance matrix is set diagonal as described in Sect.3 in order to reduce the computing time. ~~100~~110 % of a typical profile is used to build the a priori covariance matrix with 3 km vertical correlation between the adjacent pressure levels by a parametric ~~Gaussian~~ exponential function. The true profiles are defined with a vertical resolution of 0.5 km. The true species profiles are multiplied by a factor of 1.1 to be the a priori profiles, and the true temperature profile is added a 5 K offset to be the a priori profile. ~~The retrieval grid resolution is 1 km below 25 km, 2.5 km below 50 km, and 5 km above 50 km.~~ The molecules are retrieved simultaneously from each band.

The expected 1σ noise is calculated by Eq. (9), and ~~thus~~ the noise is assumed to be ~~2~~2.2 K, ~~1.7~~2.2 K, ~~1.7~~2.2 K, and ~~5~~ 5.1 K at 118, 190, 240, 640 GHz, respectively. The species such as BrO and HO_2 which emission radiances are small compared with the system noise must be averaged to increase the precision. Here the lower noise (1σ noise multiply a factor of 0.1, equivalent to a 10-degree latitude weekly zonal mean) is used to represent the averaged production.

4.2 Comparison of TALIS and Aura MLS

As discussed in section 2.2, TALIS has similar bands to Aura MLS. The major difference between these two instruments is the spectrometers used in limb sounding. A simulation is performed to compare the performance of the main products between TALIS FFT spectrometer and Aura MLS 'Standard' 25-channel spectrometer. Figure 9 to 11 show the retrieval products of TALIS and MLS, all the factors are identical except the spectrometer.

According to the simulation results, TALIS can do a better job than Aura MLS because of the wider bandwidth and finer resolution. Temperature precision of TALIS is ~~improved 1–2 K compared with~~ 1.5 K better than Aura MLS at about 15–30 km and the vertical resolution is also improved ~~about 2 km~~. The difference of precision becomes small above 50 km. H_2O precision is improved about 2–10% at about 15–50 km. O_3 precision is improved about ~~2~~3–20% at about 10–60 km. However, the Digital Autocorrelator Spectrometers of MLS which can improve the performance in the mesosphere are not considered here.

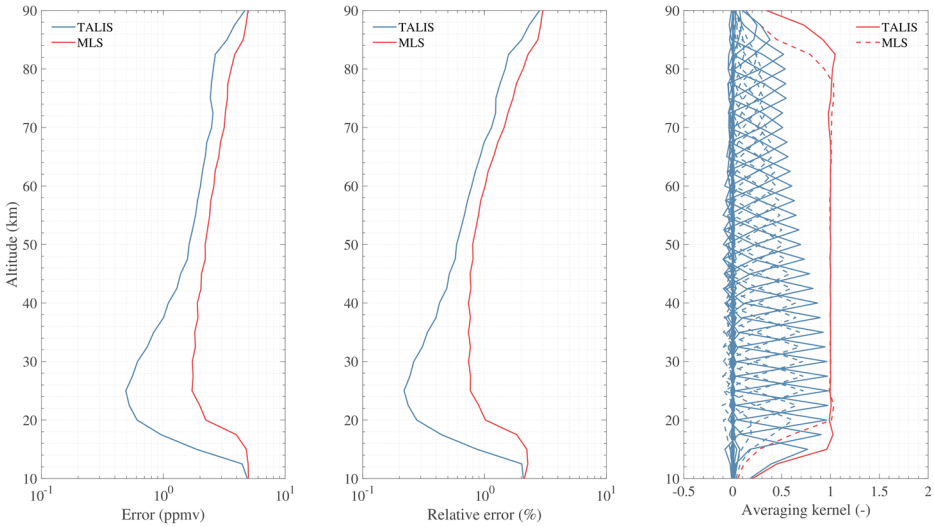

Figure 9. Temperature product comparison between TALIS FFT spectrometer and MLS 'Standard' spectrometer using 118.75 GHz line. All other factors are identical.

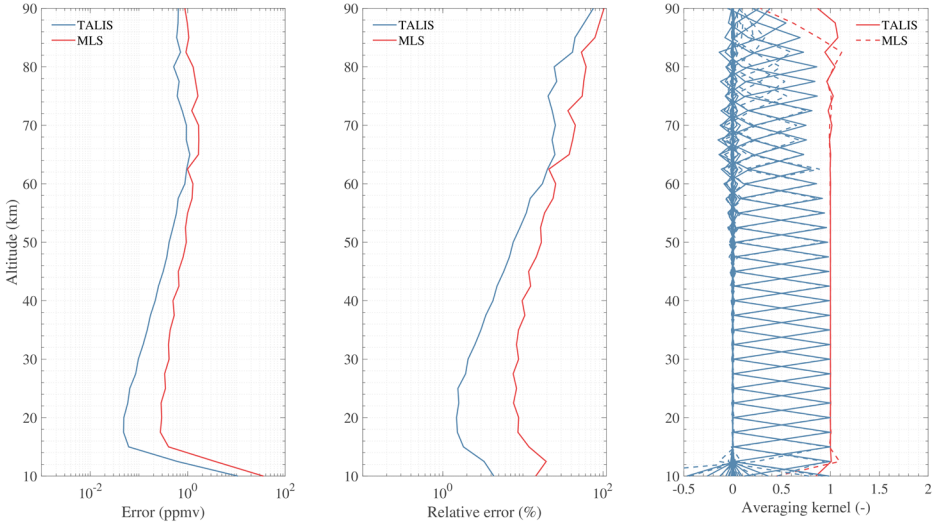

Figure 10. H_2O product comparison between TALIS FFT spectrometer and MLS 'Standard' spectrometer using 183.31 GHz line. All other factors are identical.

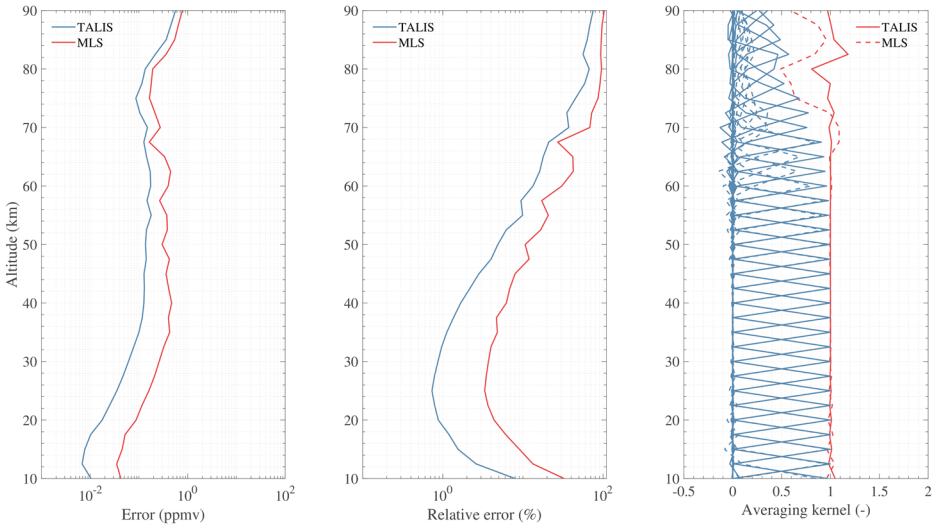

Figure 11. O_3 product comparison between TALIS FFT spectrometer and MLS 'Standard' spectrometer using 235.71 GHz line. All other factors are identical.

4.3 Retrieval precision

Since the simulation has been performed, an evaluation of the retrieval precision on the target species of TALIS is made. Retrieval profile, a priori profile, and true profile are all plotted in Figs. 12 to 28. The precision (square root of diagonal elements of the error covariance matrix) is given for a single scan and averaged measurement respectively, and the relative error is also provided. Auxiliary information about averaging kernel function and measurement response are also included. Results are discussed in details in the followings.

4.3.1 ~~High~~ Better precision products

Temperature, H_2O, O_3, HNO_3, HCl, N_2O, and ClO are treated as ~~high~~ better precision products because of the good precision for a single scan measurement. These products can be used in scientific research directly.

Atmospheric temperature is the most important parameter that can be retrieved with high signal-noise ratio in lower frequency or good vertical resolution in high frequency by using O_2 lines. TALIS will use 118 GHz radiometer to detect atmospheric temperature profile, with 240 and 643 GHz radiometers worked as supplement products. Results are shown in Fig. 12, the sensitivity is significantly high at the 118 GHz band. Single scan precision is ~~< 1K from 25 to 45 km and < 2K at other useful range~~ good from 15 to 60 km with the precision < 2 K. The retrieval vertical resolution is 2.5-4 km below 50 km and ~~5~~4–6 km from 50 to 80 km. The precision of averaged measurement will be < 1 K from 15 to 85 km.

'Wide' filters of MLS make measurements extending down into the troposphere~~, and TALIS is lack of the information~~ where TALIS lacks sensitivity. However, ~~the retrieval precision of 240 GHz band is better in the upper troposphere and~~ the

240 GHz product can compensate for the loss of information since the precision is better in the upper troposphere (error < 1 K for a vertical resolution of 2.5-3 km between 10 and 15 km). Result of 643 GHz band ~~looks~~ is similar to that of 240 GHz band.

Once the temperature profile is retrieved, the pressure profile can be calculated from the hydrostatic equilibrium equation using a known pressure and temperature at a reference tangent point. The pressure profile is not a direct product and is not shown here.

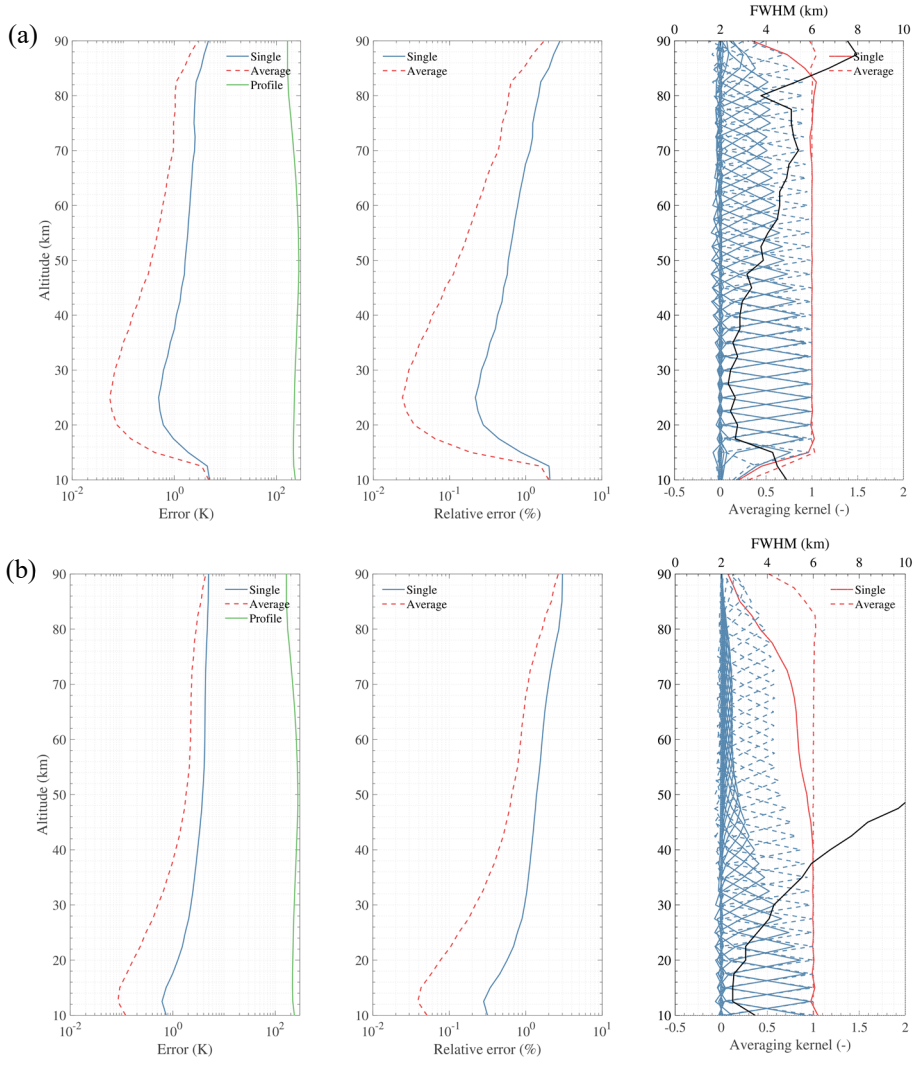

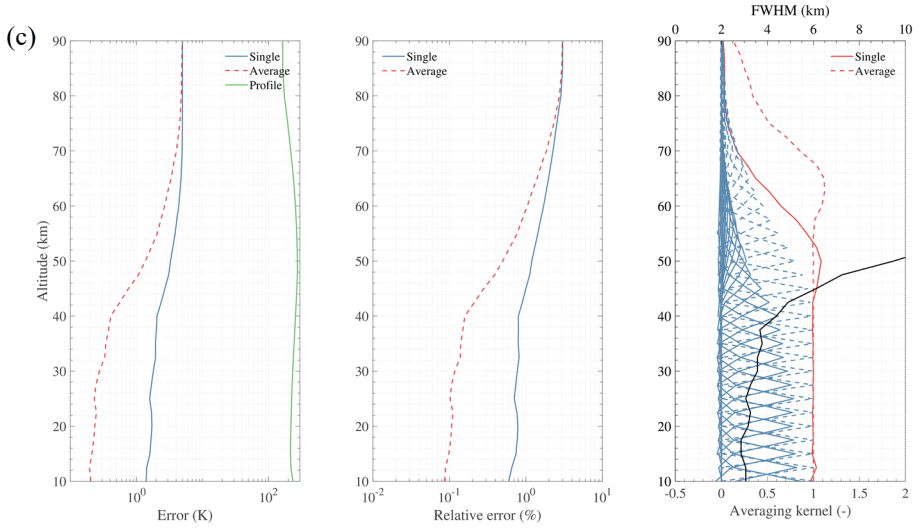

Figure 12. Simulation results of temperature retrieval using 118.75 (a), 233.95 (b), and 627.75 GHz (c) lines. Single and Average represent the retrieval error using different noise. Profile represent the typical profile used in simulation. The black solid line in the last panel represent the FWHM (i.e. vertical resolution).

The H_2O profile, another key parameter, can be measured by 190 and 643 GHz radiometers. The 183.31 GHz line is generally used by humidity sounder to detect water vapour with ~~high~~ good precision. Figure 13 shows the retrieval precision will be < 10% from ~~25~~ 10 to ~~75~~ 55 km by 190 GHz single scan measurement with the vertical resolution of 2.5–~~5~~ 4 km. Averaged measurement has the retrieval precision < 1% at ~~25–80~~ 10–55 km, < ~~20~~5% at ~~other effective altitudes~~10–80 km. The profile can also be retrieved by 643 GHz radiometer with ~~less~~ poorer precision.

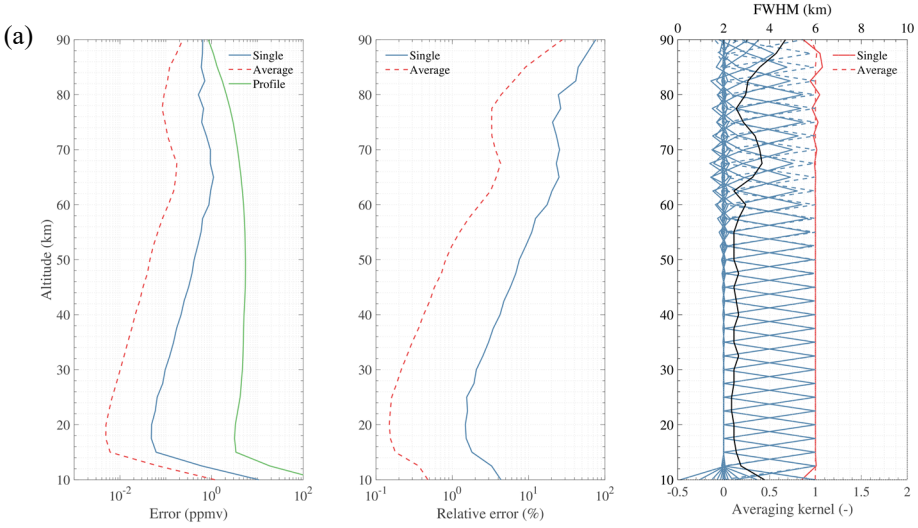

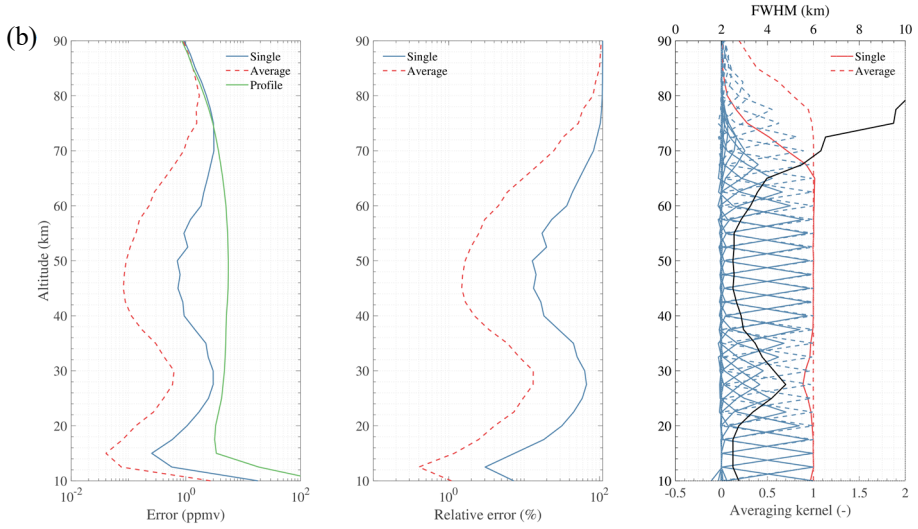

Figure 13. Simulation results of H_2O retrieval using 183.31 (a) and 657.9 GHz (b) lines. Single and Average represent the retrieval error using different noise. Profile represent the typical profile used in simulation. The black solid line in the last panel represent the FWHM (i.e. vertical resolution).

O_3 has quite strong intensity in most spectral regions of TALIS. All the radiometers except 118 GHz can be used to observe this gas which is important for energy balance (Fig. 14). The 240 GHz radiometer which covers the 235.7 GHz line has the highest O_3 sensitivity. The profile can be retrieved with a single scan precision < ~~5~~10% from ~~25~~ 10 to ~~60~~ 55 km and the vertical resolution is 2.5–3 km. The vertical resolution will degrade to ~~5–8~~3–6 km for altitudes higher than ~~60~~ 70 km. By averaging the measurements, the precision will be < ~~1~~5% at ~~25–65~~10–70 km. The other two bands show good performance from ~~25~~ 15 to ~~60~~ 55 km with a single scan precision < ~~5~~10%.

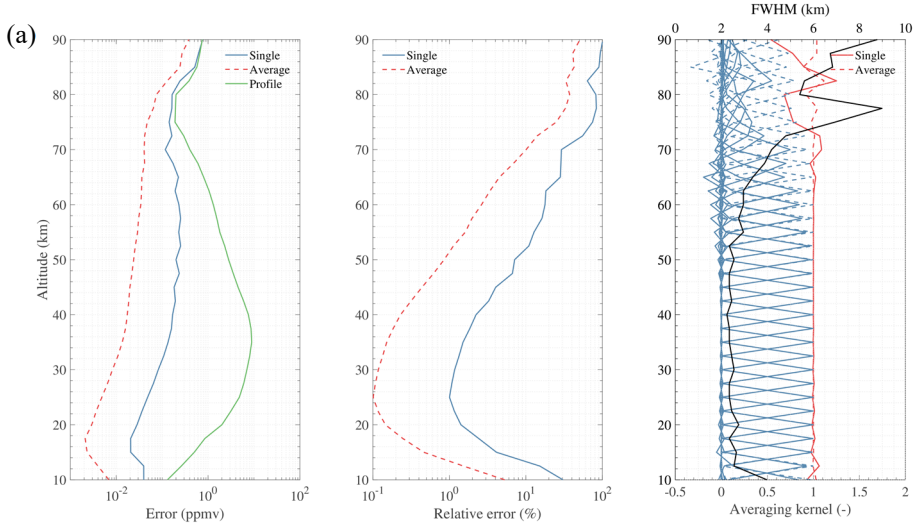

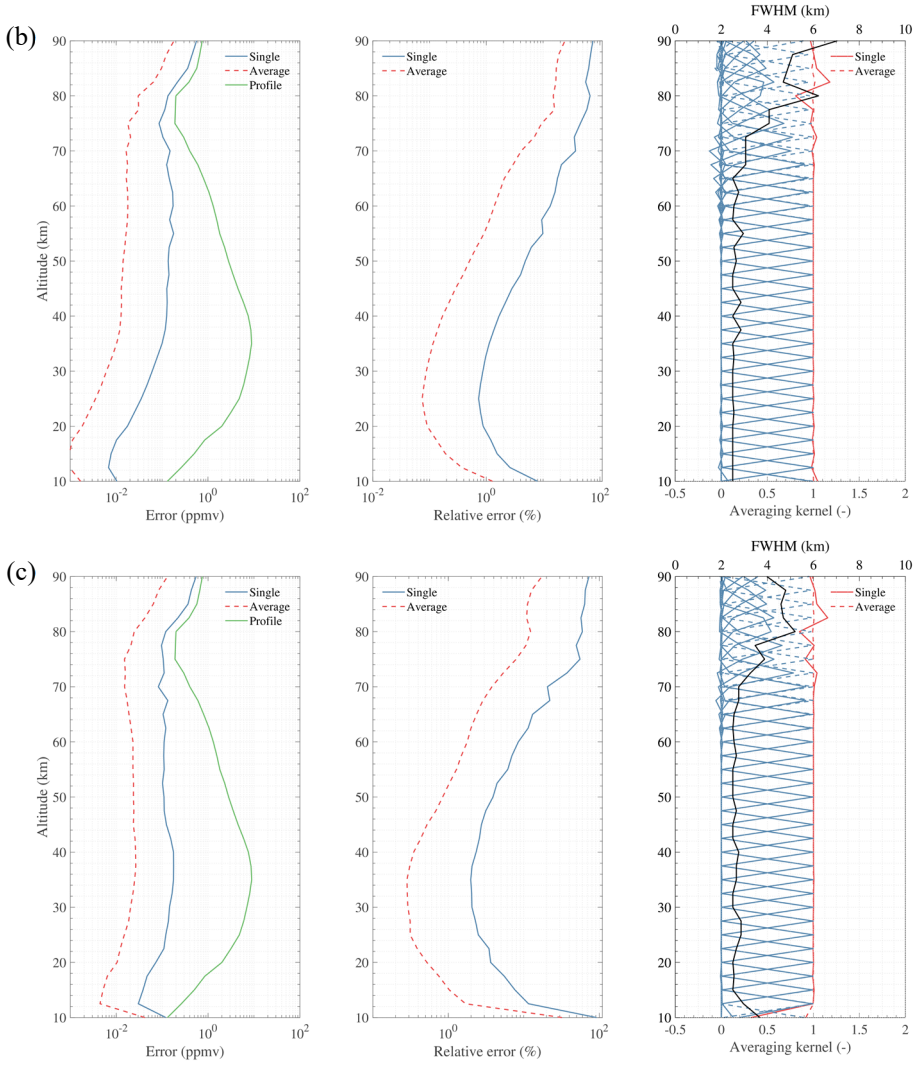

Figure 14. Simulation results of O_3 retrieval using 190 (a), 235.7 (b), and 657.5 GHz (c) lines. Single and Average represent the retrieval error using different noise. Profile represent the typical profile used in simulation. The black solid line in the last panel represent the FWHM (i.e. vertical resolution).

HNO_3 is a common species in the stratosphere and has relatively strong lines at 240 and 643 GHz bands. Figure 15 shows the results of HNO_3 retrieval. The 240 GHz radiometer can measure HNO_3 at ~~25–35~~15–32 km altitude range with a single scan precision < 30% and the vertical resolution is 2.5–~~5~~ 3 km ~~through most of the useful range~~. Averaging the measurements can improve the retrieval with a precision < 10% from ~~25~~ 15 to 35 km. The 643 GHz signal is stronger than that in the 240 GHz band, but it is strongly absorbed by O_3 below about 30 km. However, after averaging the measurements, information can be retrieved between ~~25~~ 15 and 70 km with a precision better than ~~50~~60%.

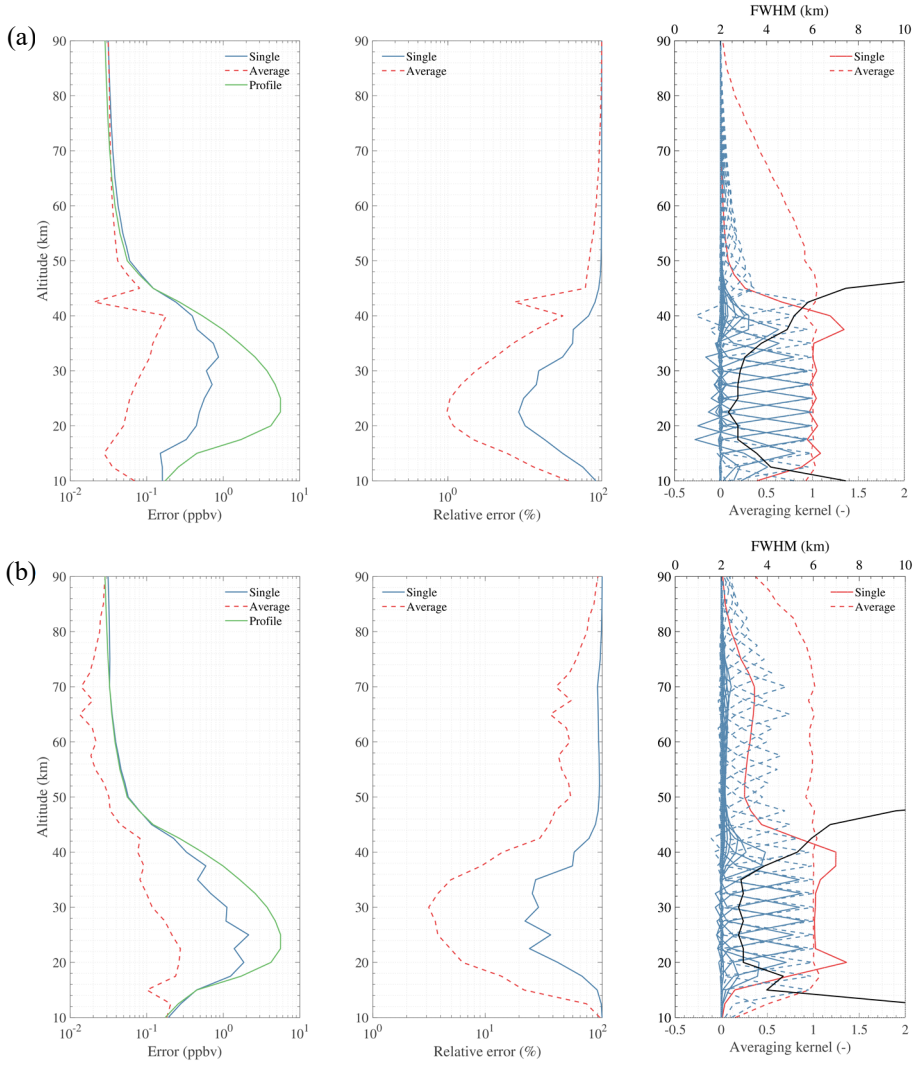

Figure 15. Simulation results of HNO_3 retrieval using 244 (a), and 656 GHz (b) lines. Single and Average represent the retrieval error using different noise. Profile represent the typical profile used in simulation. The black solid line in the last panel represent the FWHM (i.e. vertical resolution).

Figure 16 shows the expected precision of HCl observation. HCl can be measured at ~~25~~15–50 km with < 20% single scan relative error with the vertical resolution of 2.5–~~5~~ 3 km ~~through most of the useful range~~. By averaging the measurements, the precision will be < ~~5~~10% at ~~25–65~~12–72 km.

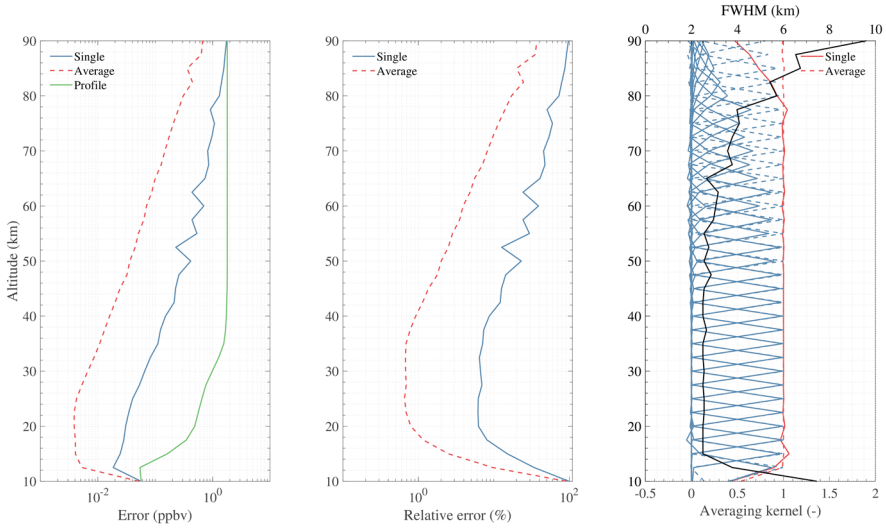

Figure 16. Simulation result of HCl retrieval using 624.9 GHz lines. Single and Average represent the retrieval error using different noise. Profile represent the typical profile used in simulation. The black solid line in the last panel represent the FWHM (i.e. vertical resolution).

N_2O can be retrieved from the band at 190 GHz in the upper troposphere while the band at 643 GHz can provide more information and good precision in the stratosphere. Figure 17 shows that single scan precision of 190 GHz is < ~~40~~20% at ~~10–35~~12–32 km with the vertical resolution of 2.5~~–5~~ km. By averaging the measurements, the precision will be < ~~30~~10% from 10 to ~~45~~ 42 km. The ~~643~~ 190 GHz can give the similar precision at ~~15–50~~10–20 km.

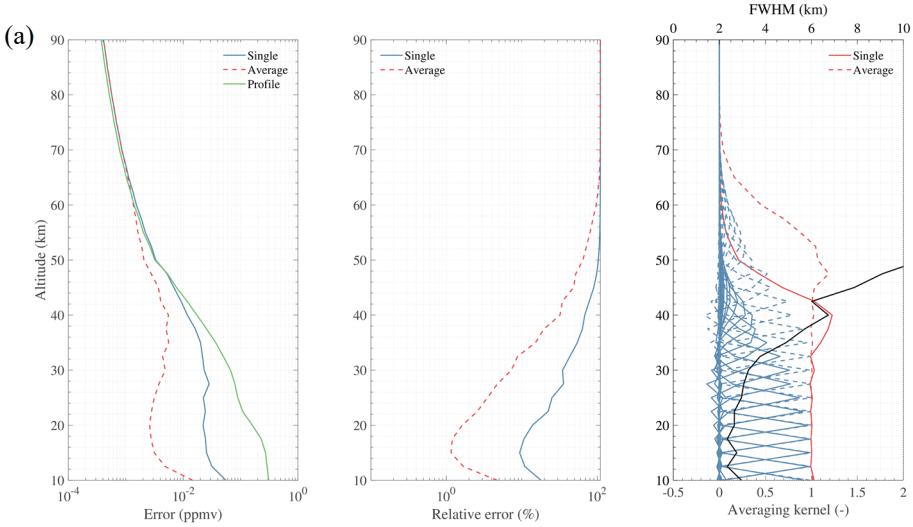

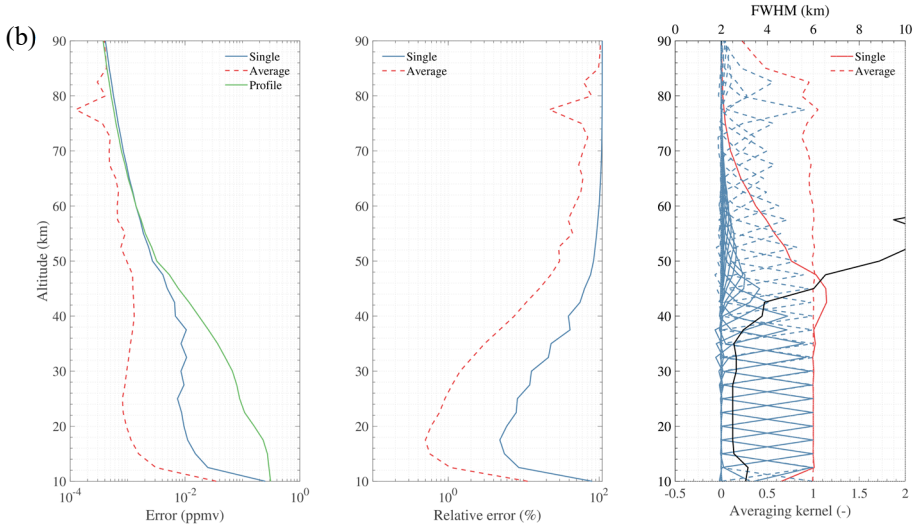

Figure 17. Simulation results of N_2O retrieval using 200.98 (a), and 652.834 GHz (b) lines. Single and Average represent the retrieval error using different noise. Profile represent the typical profile used in simulation. The black solid line in the last panel represent the FWHM (i.e. vertical resolution).

ClO can be retrieved from radiances measured by 190 and 643 GHz bands (Fig. 18). However, the result shows that the best retrievals are performed from the band at 643 GHz but information can also be retrieved from the 190 GHz radiometer with ~~less~~ poorer precision. Single scan measurement from 643 GHz radiometer can be used to obtain ClO with ~~30–50~~< 40% precision from 30 to 45 km, and the vertical resolution is about ~~3~~2.5–4 km throughout the useful range. By averaging the measurements, precision will be ~~5–~~< 30% from ~~25~~ 23 to ~~60~~ 57 km. Since ClO will vanishes in the middle stratosphere (30-40 km) during nighttime, the precision will be worse in the nighttime. In the polar regions, the relative precision will be better between 20 and 25 km during chlorine activation.

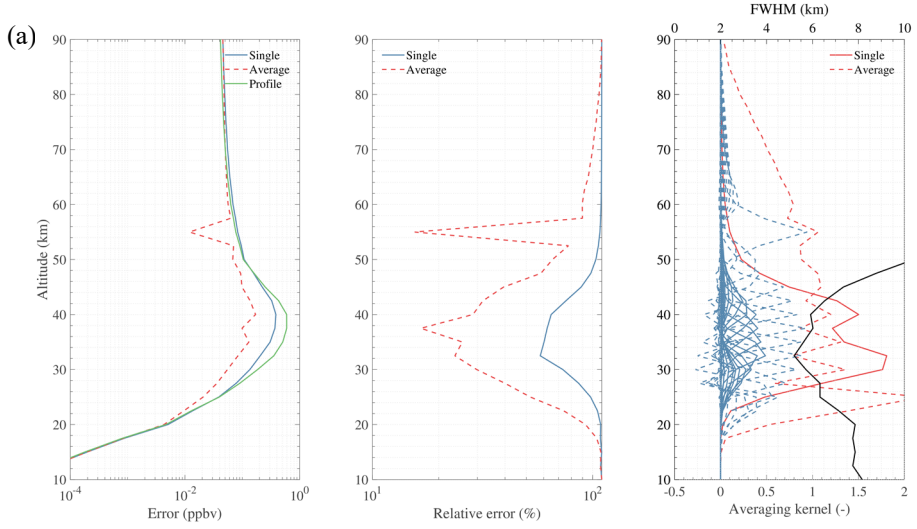

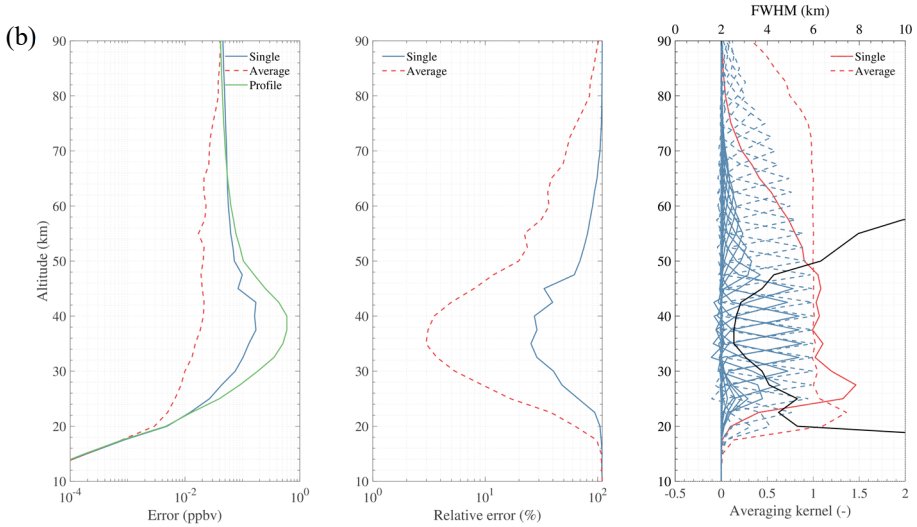

Figure 18. Simulation results of ClO retrieval using 203.4 (a) and 649.45 GHz (b) lines. Single and Average represent the retrieval error using different noise. Profile represent the typical profile used in simulation. The black solid line in the last panel represent the FWHM (i.e. vertical resolution).

4.3.2 Medium precision products

Medium precision products including CO, HCN, CH_3Cl mean that their single scan retrieval precisions are not satisfying, but can be used to some degree. There is a choice for the user to select the single scan or averaged products.

CO can be measured using 230.538 and 661.07 GHz lines. Figure 19 shows that the 240 GHz radiometer can provide CO information with ~~40~~30–90% single scan precision from 10 to ~~70~~ 90 km. The vertical resolution is in the range 3.5–5.5 km from the upper troposphere to the lower mesosphere, degrading to 6–10 km in the upper mesosphere. By using averaged measurements, CO can be retrieved with ~~< 40% relative error from 10 to 25 km, ~~< ~~20~~30% relative error at the range of ~~25–95~~10–90 km. However, the retrieval of 643 GHz measurement shows poor precision.

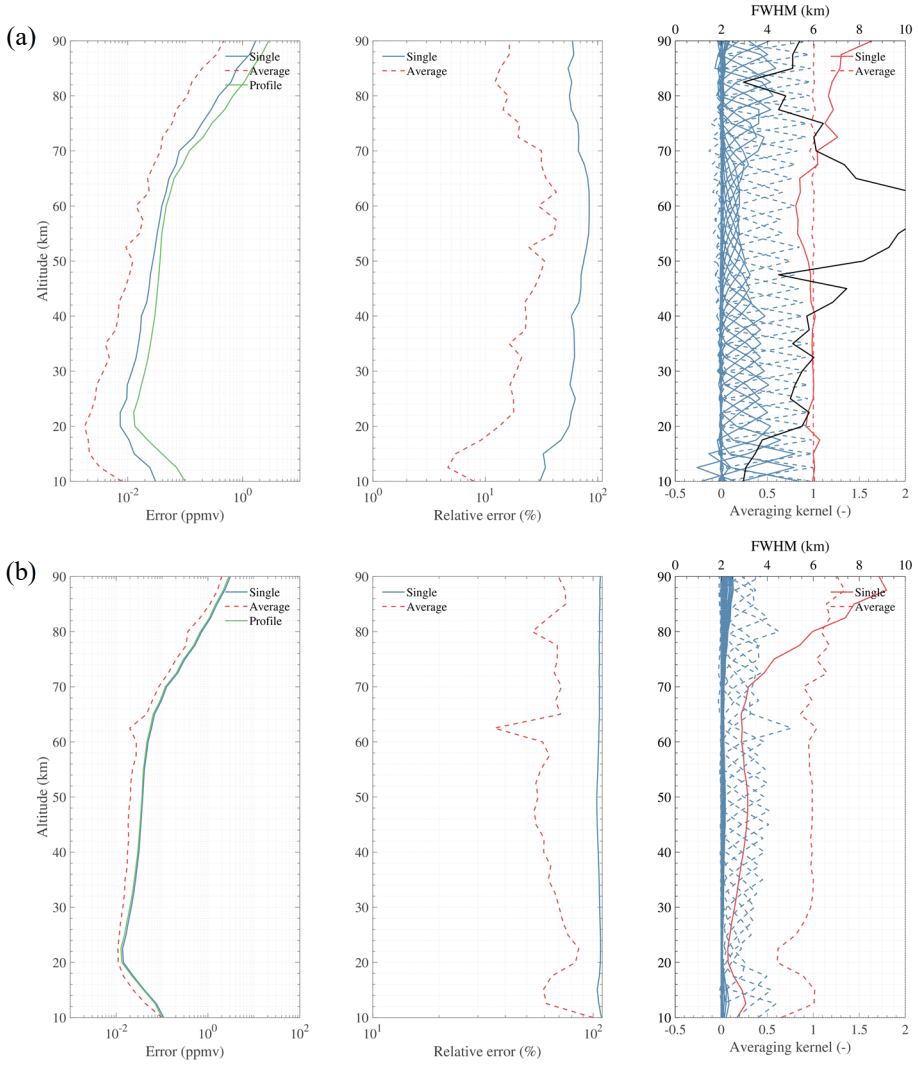

Figure 19. Simulation results of CO retrieval using 230.538 (a) and 661.07 GHz (b) lines. Single and Average represent the retrieval error using different noise. Profile represent the typical profile used in simulation. The black solid line in the last panel represent the FWHM (i.e. vertical resolution).

HCN is measured by 190 GHz radiometer at 177.26 GHz line. The single scan precision is ~~around~~ < 50% from ~~18~~ 12 to ~~32~~ 28 km and the vertical resolution is about 5 km at the height of 30 km, degrading to 8 km at about 40 km (Fig. 20). By averaging the measurements, the relative error will be < ~~50~~30% at ~~15~~10 ~~60~~ 40 km.

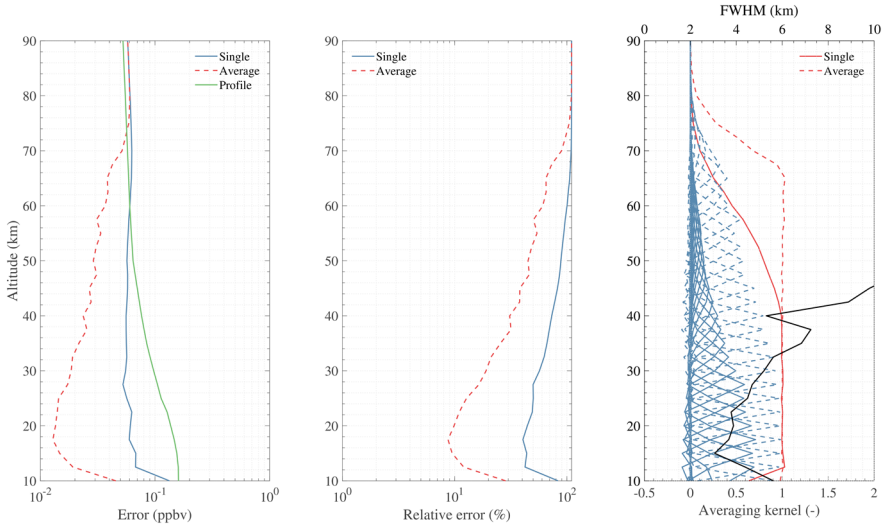

Figure 20. Simulation result of HCN retrieval using 177.26 GHz line. Single and Average represent the retrieval error using different noise. Profile represent the typical profile used in simulation. The black solid line in the last panel represent the FWHM (i.e. vertical resolution).

CH_3Cl can be measured by the 643 GHz radiometer. As the result shows (Fig. 21), the 649.5 GHz band are suitable for CH_3Cl observation in the upper troposphere and lower stratosphere. It can be measured with ~~40–50~~< 30% single scan precision from ~~15–~~12 to 23 km, with ~~20–50~~< 20% averaged precision from ~~12–~~10 to 30 km. The vertical resolution is about 3 ~~–~~4 km over most of the useful range.

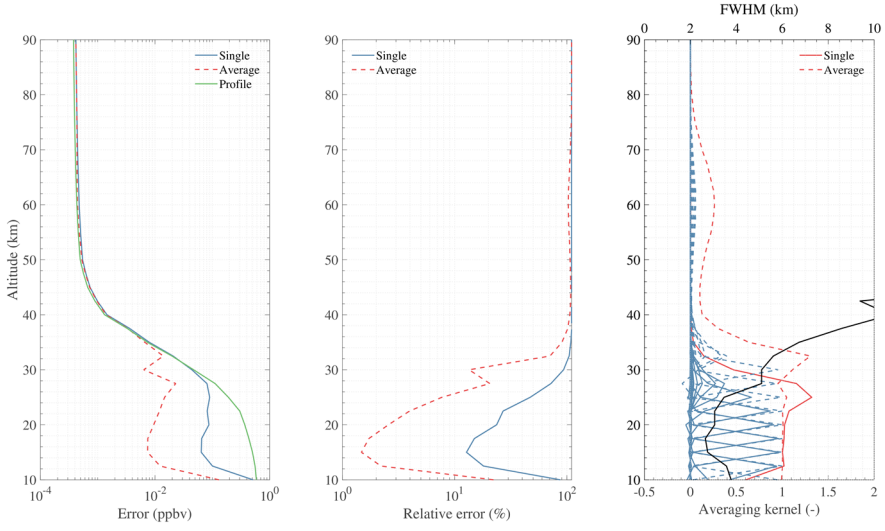

Figure 21. Simulation results of CH_3Cl retrieval using 649.5 GHz lines. Single and Average represent the retrieval error using different noise. Profile represent the typical profile used in simulation. The black solid line in the last panel represent the FWHM (i.e. vertical resolution).

4.3.3 ~~Low~~ Poor precision products

There are several weak lines in the spectral regions of TALIS such as HOCl, BrO, and HO_2. ~~Significantly average~~ Significant averaging must be done to these measurements in order to obtain reliable and satisfying precision.

The 635.87 GHz line is the most appropriate line for HOCl observation. However, the single scan retrieval has poor precision of ~~70–100~~60–80% at 25–45 km with the vertical resolution of about ~~4–~~6 km. Figure 22 reveals that HOCl can be retrieved from ~~22~~ 20 to ~~52~~ 50 km with averaged measurement precision of ~~15 <~~ 50%.

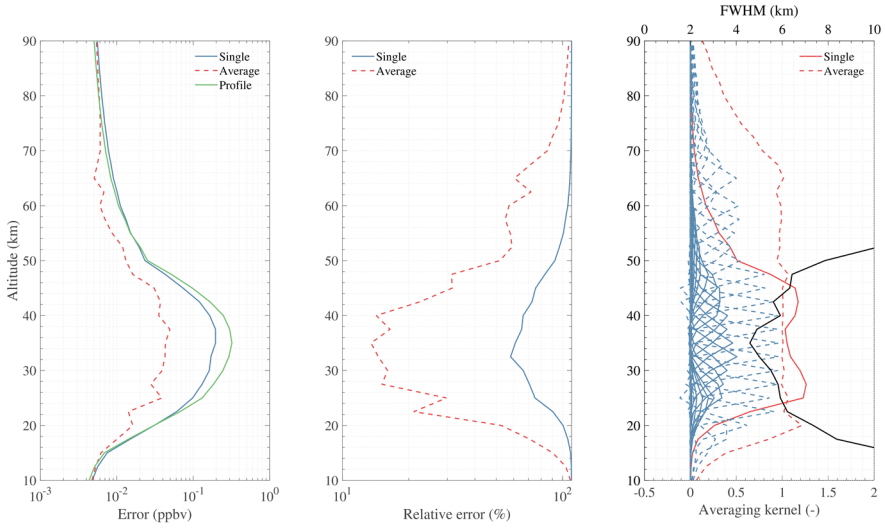

Figure 22. Simulation result of HOCl retrieval using 635.87 GHz line. Single and Average represent the retrieval error using different noise. Profile represent the typical profile used in simulation. The black solid line in the last panel represent the FWHM (i.e. vertical resolution).

BrO can be measured by using 624.768 GHz spectral line. Figure 23 shows the simulation result of BrO retrieval. As the averaging kernel reveals, there is almost no useful information in single scan measurement because of the quite poor signal-to-noise ratio. Therefore, averaging is needed to obtain reliable and scientific results. The error is ~~50–80~~ 50% from ~~23~~ 24 to ~~56~~ 48 km with the vertical resolution of about 4 km.

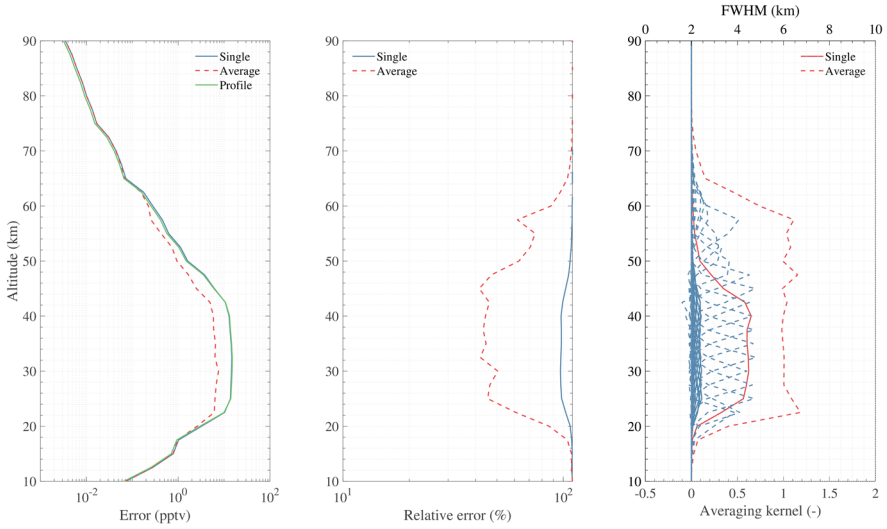

Figure 23. Simulation results of BrO retrieval using 624.768 GHz line. Single and Average represent the retrieval error using different noise. Profile represent the typical profile used in simulation. The black solid line in the last panel represent the FWHM (i.e. vertical resolution).

HO_2 can be measured by the 643 GHz radiometer with ~~10 –~~ < 50% precision at the vertical range of ~~35–85~~30–90 km by using averaged data (Fig. 24). The precision of single scan retrieval is 55–70% at 40–75 km which is not desirable because of the weak signal. The vertical resolution is about 6 km.

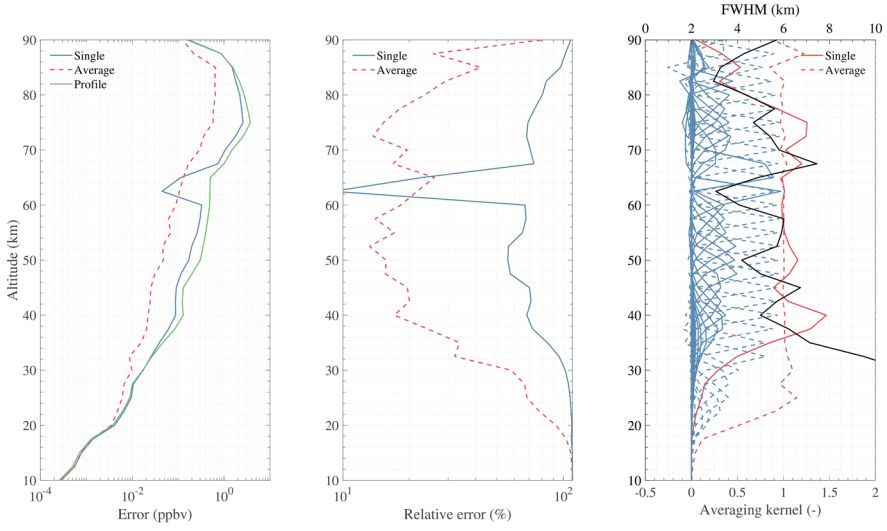

Figure 24. Simulation results of HO_2 retrieval using 649.701 GHz line. Single and Average represent the retrieval error using different noise. Profile represent the typical profile used in simulation. The black solid line in the last panel represent the FWHM (i.e. vertical resolution).

4.3.4 Promising products

The unique products are the target species which are not covered by Aura MLS but covered by TALIS. There are four gases: NO, NO_2, H_2CO, and SO_2 (normal VMR). However, their signals all have weak intensity and must be averaged to improve the retrieval precision.

NO (daytime) can be retrieved from averaged data with ~~10–40~~< 50% precision at ~~30–95~~28–90 km (Fig. 25) while it vanishes in the nighttime. The vertical resolution is about ~~6~~ 4–10 km. While its single scan measurement has no information in the area where NO largely exists.

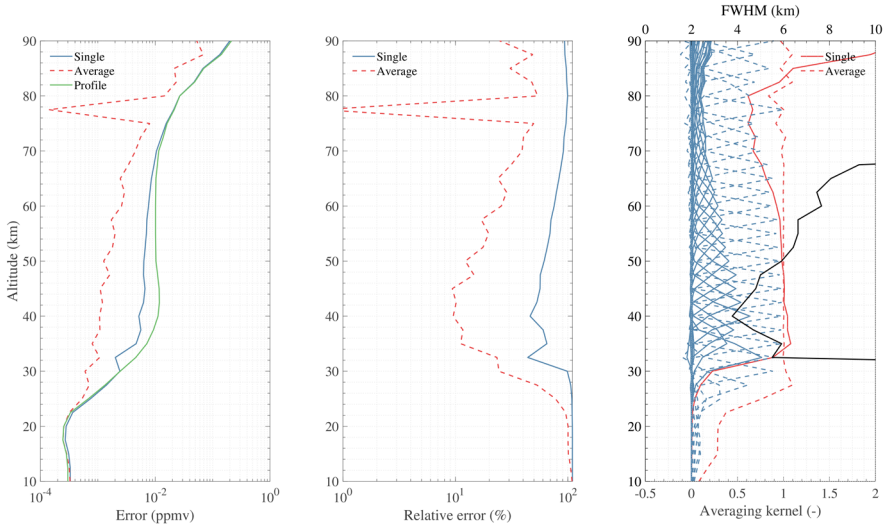

Figure 25. Simulation result of NO retrieval using 651.75 GHz line. Single and Average represent the retrieval error using different noise. Profile represent the typical profile used in simulation. The black solid line in the last panel represent the FWHM (i.e. vertical resolution).

NO_2 (nighttime) has a weak line in the spectrum of 240 GHz band and it vanishes in the daytime. Figure 26 shows that only averaged measurement can provide some information at ~~25~~20–40 km with the precision of about ~~50~~40–60 % in the nighttime. The vertical resolution is about 5 km.

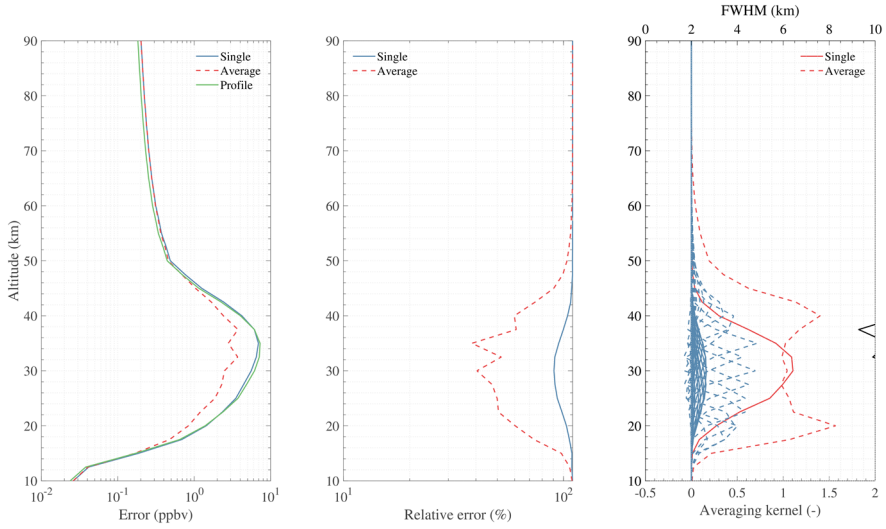

Figure 26. Simulation result of NO_2 retrieval using 232.7 GHz lines. Single and Average represent the retrieval error using different noise. Profile represent the typical profile used in simulation. The black solid line in the last panel represent the FWHM (i.e. vertical resolution).

Although H_2CO has a line at 656.45 GHz, its emission radiance is too weak. Almost no useful information can be obtained (Fig. 27). However, this line has the potential to measure H_2CO. More average or other effective methods should be applied to get acceptable precision.

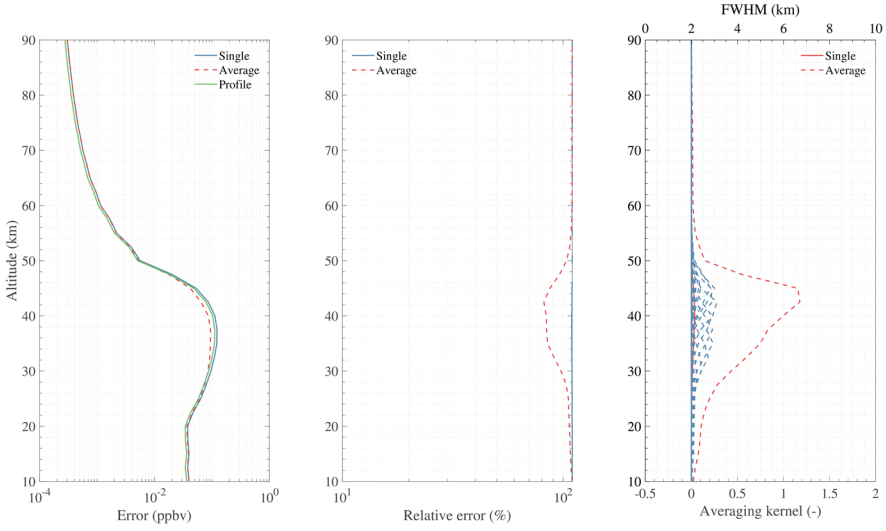

Figure 27. Simulation result of H_2CO retrieval using 656.45 GHz line. Single and Average represent the retrieval error using different noise. Profile represent the typical profile used in simulation. The black solid line in the last panel represent the FWHM (i.e. vertical resolution).

MLS standard SO_2 product is taken from the 240 GHz retrieval, but only effective when its concentration significantly enhanced. TALIS has both 240 and 643 GHz radiometer which covering the lines of SO_2. The 240 GHz radiometer can be used to measure SO_2 like the way of MLS. The 643 GHz radiometer can give the concentration of nominal background. The averaged result shows that SO_2 can be retrieved at 14–20 km, ~~40–75~~46–70 km with the relative error about ~~20–60~~< 50% (Fig. 28). The vertical resolution is about 6 km.

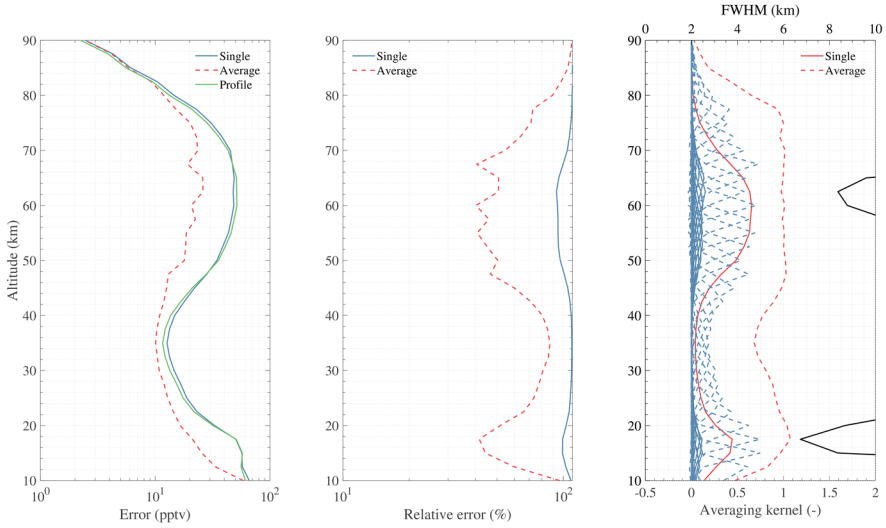

Figure 28. Simulation result of SO_2 retrieval using 659 GHz lines. Single and Average represent the retrieval error using different noise. Profile represent the typical profile used in simulation. The black solid line in the last panel represent the FWHM (i.e. vertical resolution).

5 Conclusions

Simulation analysis for temperature and chemical species retrieval have been performed to assess the measurement performance of TALIS and to support the mission. This study mainly focuses on a large number of important chemical species in middle and upper atmosphere which can be observed by limb sounder. The results are summarized in Table 3.

~~The results of seven high sensitivity products are reliable~~ Seven species show high sensitivity, sufficient for scientifically useful single profile retrievals. 118, 240, and 643 GHz observations of O_2 are used to estimate temperature profile which is quite important in meteorology. The 118 GHz radiometer can obtain temperature with a precision < 2 K at 15–80 km and the 240 and 643 GHz radiometers can provide information in the upper troposphere. The 190 GHz radiometer can be used to measure H_2O with a precision < 10% in a wide vertical range and give information of upper tropospheric humidity. O_3 can be measured by three radiometers, and the 240 GHz radiometer has the best precision. The precision is < 5% from 25 to 60 km by single scan measurement. HNO_3 can be derived from 240 GHz retrieval with a precision < 40%. The precision of HCl single scan retrieval is < 40% over most of the useful range. The 190 GHz radiometer can give a good estimate to N_2O

profile with a precision about 20–40%, while 643 GHz measurement can provide more information at higher altitudes. Single scan precision of ClO measured by 643 GHz radiometer is about 30% in the area where ClO mainly exists. CH_3Cl can be measured in the upper troposphere and low stratosphere with a precision about 50%. The profile of CO retrieved from 240 GHz measurement is better than that from 643 GHz measurement. The best sensitivity is found between 70~90 km where the VMR of CO is large, and the precision is better than 50%. HCN have 50% single scan precision at 18–32 km which may need to be averaged. Other measurements such as HO_2, HOCl, NO, NO_2, BrO, SO_2, and H_2CO must be significantly averaged before scientific use because of the weak signals. As the results show that the precision of some products become much poorer suddenly at a height of 25 km, it seems that the retrieval grid resolution does not match the achievable resolution.

Apart from these products, some potential products will be discussed in the future works. Line-of-sight wind is important information which could be measured by TALIS. Cloud IceWater Content (IWC) is also an essential product provided by passive microwave radiometer. Future studies will also investigate the Zeeman effect as it polarizes and changes the shape of the O_2 lines.

TALIS has strong potential to monitor chemical composition in the whole Earth's atmosphere which is important for numerical weather prediction models and to characterize the long-time change of climate. Measurement data can be used for atmospheric chemistry and dynamics study which is quite important for the geoscience. A better understanding of the key chemical and dynamical processes in the middle and upper atmosphere will help us solve the climate problem more efficient.

This paper is the preliminary analysis of the instrument. More studies such as structure optimization, calibration research, and error analysis will be performed to support the mission.

Table 3. Simulation results of TALIS retrieval precision

Product	Radiometer	Single precision	Average precision
Temperature	118 GHz, 240 GHz	< 2K (10–~~75~~ 60 km)	< ~~1K~~ 2K (10–85 km)
H_2O	190 GHz	< 10% (~~25–75~~10–55 km)	~~–~~ < ~~1~~5% (~~25~~10–80 km)
O_3	240 GHz	< ~~5~~10% (~~25~~10–55 km)	~~–~~ < ~~1~~5% (~~25~~10–70 km)
HCl	643 GHz	~~10–50~~ < 20% (15–~~70~~ 50 km)	< 10% (~~25~~12–~~75~~ 72 km)
N_2O	~~190 GHz,~~ 643 GHz	~~20–40~~ < 20% (~~10–40~~12–32 km)	< ~~40~~10% (10–~~50~~ 42 km)
HNO_3	240 GHz	~~10–50~~ < 30% (15–~~35~~ 32 km)	< ~~50~~10% (~~10~~15–~~45~~ 35 km)

ClO	643 GHz	~~30–50~~< 40% (30–45 km)	< 30% (~~25~~23–~~60~~57 km)
CO	240 GHz	~~40~~30–90% (10–~~70~~90 km)	< ~~40~~30% (10–~~95~~90 km)
HCN	190 GHz	~~20–~~< 50% (~~18~~12–~~32~~ 28 km)	~~10–50~~< 30% (~~15~~10–~~60~~40 km)
CH_3Cl	643 GHz	~~40–50~~< 30% (~~15~~12–23 km)	~~20–50~~< 20% (~~12~~10–30 km)
HOCl	643 GHz	~~70–90~~60–80% (~~27–43~~25–45 km)	~~15–~~< 50% (~~22–52~~20–50 km)
BrO	643 GHz	/	~~50–80~~< 50% (~~23–56~~ 24–48 km)
HO_2	643 GHz	~~60–80~~< 70% (~~47–67~~40–75 km)	~~10–~~< 50% (~~35–85~~30–90 km)
NO	643 GHz	~~60–80~~50–70 % (33–55 km)	~~10–40~~< 50% (~~30–95~~28–90 km)
NO_2	240 GHz	/	~~50~~40–60% (~~25~~20–40 km)
H_2CO	643 GHz	/	/
SO_2	643 GHz	/	~~20–60~~< 50% (~~40–75~~14–20, 46–70 km)

Code and data availability. ARTS can be downloaded at http://www.radiativetransfer.org/getarts/. Qpack is included in the Atmlab which can be downloaded from http://www.radiativetransfer.org/tools/. Profiles and spectroscopy data of Perrin and HITRAN are included in ARTS XML Data. JPL molecular spectroscopy catalogue is available at https://spec.jpl.nasa.gov/. MLS version 4.2 data can be obtained at https://doi.org/10.5067/Aura/MLS/DATA3020.

Author contribution. Zhenzhan Wang designed the mission concept. Wenyu Wang performed the simulate and wrote the manuscript. Wenyu Wang and Yongqiang Duan analysed the results. Zhenzhan Wang edited the article.

Competing interests. The authors declare that they have no conflict of interest.

Acknowledgements. The authors would like to thank the ARTS and Qpack development teams for assistance configuring and running the model. The authors thank the JPL for providing spectroscopy data and MLS data. They would also like to thank the reviewers and the editors for their valuable and helpful suggestions.

References

Barath, F. T., Chavez, M. C., Cofield, R. E., Flower, D. A., Frerking, M. A., Gram, M. B., Harris, W. M., Holden, J. R., Jarnot, R. F., Kloezeman, W. G., Klose, G. J., Lau, G. K., Loo, M. S., Maddison, B. J., Mattauch, R. J., McKinney, R. P., Peckham, G. E., Pickett, H. M., Pickett, G., Soltis, F. S., Suttie, R. A., Tarsala, J. A., Waters, J. W., Wilson, W. J.: The Upper Atmosphere Research Satellite microwave limb sounder instrument, J. Geophys. Res.-Atmos., 98, 10751-10762, https://doi.org/10.1029/93JD00798, 1993.

Baron, P., Ricaud, P., de la Nöe, J., Eriksson, P., Merino, F., Ridal, M., and Murtagh, D. P.: Studies for the Odin Sub-Millimetre Radiometer. II. Retrieval methodology, Can. J. Phys., 80, 341–356, https://doi.org/10.1139/P01-150, 2002.

Baron, P., Urban, J., Sagawa, H., Möller, J., Murtagh, D. P., Mendrok, J., Dupuy, E., Sato, T. O., Ochiai, S., Suzuki, K., Manabe, T., Nishibori, T., Kikuchi, K., Sato, R., Takayanagi, M., Murayama, Y., Shiotani, M., and Kasai, Y.: The Level 2 research product algorithms for the Superconducting Submillimeter-Wave Limb-Emission Sounder (SMILES), Atmos. Meas. Tech., 4, 2105-2124, https://doi.org/10.5194/amt-4-2105-2011, 2011.

Baron, P., Murtagh, D. P., Urban, J., Sagawa, H., Ochiai, S., Kasai, Y., Kikuchi, K., Khosrawi, F., Körnich, H., Mizobuchi, S., Sagi, K., and Yasui, M.: Observation of horizontal winds in the middle-atmosphere between 30°S and 55°N during the northern winter 2009–2010, Atmos. Chem. Phys., 13, 6049–6064, https://doi.org/10.5194/acp-13-6049-2013, 2013.

Baron, P., Murtagh, D., Eriksson, P., Mendrok, J., Ochiai, S., Pérot, K., Sagawa, H., and Suzuki, M.: Simulation study for the Stratospheric Inferred Winds (SIW) sub-millimeter limb sounder, Atmos. Meas. Tech., 11, 4545-4566, https://doi.org/10.5194/amt-11-4545-2018, 2018.

Bremer, J. C.: Improvement of Scanning Radiometer Performance by Digital Reference Averaging, IEEE. T. INSTRUM. MEAS., 28, 46–54, https://10.1109/TIM.1979.4314759, 1979.

Eriksson, P., Jiménez, C., and Buehler, S. A.: Qpack, a general tool for instrument simulation and retrieval work, J. Quant. Spectrosc. Ra., 91, 47–64, https://doi.org/10.1016/j.jqsrt.2004.05.050, 2005.

Eriksson, P., Ekström, M., Melsheimer, C., and Buehler, S. A.: Efficient forward modelling by matrix representation of sensor responses, Int. J. Remote Sens., 27, 1793–1808, https://doi.org/10.1080/01431160500447254, 2006.

Eriksson, P., Ekström, M., Rydberg, B., and Murtagh, D. P.: First Odin sub-mm retrievals in the tropical upper troposphere: ice cloud properties, Atmos. Chem. Phys., 7, 471-483, https://doi.org/10.5194/acp-7-471-2007, 2007.

Eriksson, P., Buehler, S. A., Davis, C. P., Emde, C., and Lemke, O.: ARTS, the atmospheric radiative transfer simulator, Version 2, J. Quant. Spectrosc. Ra., 112, 1551–1558, https://doi.org/10.1016/j.jqsrt.2011.03.001, 2011.

Johnson, D. G., Traub, W. A., Chance, K. V., Jucks, K. W., and Stachnik, R. A.: Estimating the abundance of ClO from simultaneous remote sensing measurements of HO_2, OH, and HOCl, Geophys. Res. Lett., 22, 1869–1871, https://doi.org/10.1029/95GL01249, 1995.

Kasai, Y., Sagawa, H., Kreyling, D., Dupuy, E., Baron, P., Mendrok, J., Suzuki, K., Sato, T. O., Nishibori, T., Mizobuchi, S., Kikuchi, K., Manabe, T., Ozeki, H., Sugita, T., Fujiwara, M., Irimajiri, Y., Walker, K. A., Bernath, P. F., Boone, C., Stiller, G., von Clarmann, T., Orphal, J., Urban, J., Murtagh, D., Llewellyn, E. J., Degenstein, D., Bourassa, A. E., Lloyd, N. D., Froidevaux, L., Birk, M., Wagner, G., Schreier, F., Xu, J., Vogt, P., Trautmann, T., and Yasui, M.: Validation of stratospheric and mesospheric ozone observed by SMILES from International Space Station, Atmos. Meas. Tech., 6, 2311–2338, https://doi.org/10.5194/amt-6-2311-2013, 2013.

Kikuchi, K., Nishibori, T., Ochiai, S., Ozeki, H., Irimajiri, Y., Kasai, Y., Koike, M., Manabe, T., Mizukoshi, K., Murayama, Y., Nagahama, T., Sano, T., Sato, R., Seta, M., Takahashi, C., Takayanagi, M., Masuko, H., Inatani, J., Suzuki, M., and Shiotani, M.: Overview and early results of the Superconducting Submillimeter-Wave Limb-Emission Sounder (SMILES), J. Geophys. Res.-Atmos., 115, D23306, https://doi.org/10.1029/2010JD014379, 2010.

Lambert, A., Read, W. G., Livesey, N. J., Santee, M. L., Manney, G. L., Froidevaux, L., Wu, D. L., Schwartz, M. J., Pumphrey, H. C., Jimenez, C., Nedoluha, G. E., Cofield, R. E., Cuddy, D. T., Daffer, W. H., Drouin, B. J., Fuller, R. A., Jarnot, R. F., Knosp, B. W., Pickett, H. M., Perun, V. S., Snyder, W. V., Stek, P. C., Thurstans, R. P., Wagner, P. A., Waters, J. W., Jucks, K. W., Toon, G. C., Stachnik, R. A., Bernath, P. F., Boone, C. D., Walker, K. A., Urban, J., Murtagh, D., Elkins, J. W., and Atlas, E.: Validation of the Aura Microwave Limb Sounder middle atmosphere water vapor and nitrous oxide measurements, J. Geophys. Res.-Atmos., 112, D24S36, https://doi.org/10.1029/2007JD008724, 2007.

Lary, D. J. and Aulov, O.: Space-based measurements of HCl: Intercomparisonand historical context, J. Geophys. Res.-Atmos., 113, D15S04, https://doi.org/10.1029/2007JD008715, 2008.

Livesey, N. J. and Snyder, W. V.: EOS MLS Retrieval Processes Algorithm Theoretical Basis., Tech. Rep. JPL D-16159 / CL #04-2043, Jet Propulsion Laboratory, California Institute of Technology, Pasadena, California, 91109-8099, available at: https://mls.jpl.nasa.gov/data/eos_algorithm_atbd.pdf (last access: 26 March 2019), version 2.0, 2004.

Livesey, N. J., Filipiak, M. J., Froidevaux, L., Read, W. G., Lambet, A., Santee, M. L., Jiang, J. H., Pumphrey, H. C., Waters, J. W., Cofield, R. E., Cuddy, D. T., Daffer, W. H., Drouin, B. J., Fuller, R. A., Jarnot, R. F., Jiang, Y. B., Knosp, B. W., Li, Q. B., Perun, V. S., Schwartz, M. J., Snyder, W. V., Stek, P. C., Thurstans, R. P., Wagner, P. A., Avery, M., Browell, E. V., Cammas, J. P., Christensen, L. E., Diskin, G. S., Gao, R. S., Jost, H. J., Loewenstein, M., Lopez, J. D., Nedelec, P., Osterman, G. B., Sachse, G. W., and Webster, C. R.: Validation of Aura Microwave Limb Sounder O_3 and CO observations in the upper troposphere and lower stratosphere, J. Geophys. Res.-Atmos., 113, D15S02, https://doi.org/10.1029/2007JD008805, 2008.

Livesey, N. J., Logan, J. A., Santee, M. L., Waters, J. W., Doherty, R. M., Read, W. G., Froidevaux, L., and Jiang, J. H.: Interrelated variations of O_3, CO and deep convection in the tropical/subtropical upper troposphere observed by the Aura

Microwave Limb Sounder (MLS) during 2004–2011, Atmos. Chem. Phys., 13, 579-598, https://doi.org/10.5194/acp-13-579-2013, 2013.

Livesey, N. J., Read, W. G., Wagner, P. A., Froidevaux, L., Lambert, A., Manney, G. L., Millán, L. F., Pumphrey, H. C., Santee, M. L., Schwartz, M. J., Wang, S. H., Fuller, R. A., Jarnot, R. F., Knosp, B. W., Martinez, E., Lay, R. R.: Earth Observing System (EOS) Aura Microwave Limb Sounder (MLS) Version 4.2x Level 2 data quality and description document., Tech. Rep. JPL D-33509 Rev. D, Jet Propulsion Laboratory, California Institute of Technology, Pasadena, California, 91109-8099, available at: https://mls.jpl.nasa.gov/data/v4-2_data_quality_document.pdf (last access: 26 March 2019), Version 4.2x–3.1, 2018.

Marks, C. J. and Rodgers, C. D.: A retrieval method for atmospheric composition from limb emission measurements, J. Geophys. Res.-Atmos., 98, 14939–14953, https://doi.org/10.1029/93JD01195, 1993.

Mätzler, C.: Thermal Microwave Radiation: Applications for Remote Sensing, vol. 52, Iet, 2006.

Millán, L., Livesey, N., Read, W., Froidevaux, L., Kinnison, D., Harwood, R., MacKenzie, I. A., and Chipperfield, M. P.: New Aura Microwave Limb Sounder observations of BrO and implications for Br_y, Atmos. Meas. Tech., 5, 1741-1751, https://doi.org/10.5194/amt-5-1741-2012, 2012.

Millán, L., Wang, S., Livesey, N., Kinnison, D., Sagawa, H., and Kasai, Y.: Stratospheric and mesospheric HO_2 observations from the Aura Microwave Limb Sounder, Atmos. Chem. Phys., 15, 2889-2902, https://doi.org/10.5194/acp-15-2889-2015, 2015.

Murtagh, D., Frisk, U., Merino, F., Ridal, M., Jonsson, A., Stegman, J., Witt, G., Eriksson, P., Jimenez, C., Mégie, G., de la Nöe, J., Ricaud, P., Baron, P., Pardo, J., Hauchcorne, A., Llewellyn, E., Degenstein, D., Gattinger, R., Lloyd, N., Evans, W., McDade, I., Haley, C., Sioris, C., von Savigny, C., Solheim, B., McConnell, J., Strong, K., Richardson, E., Leppelmeier, G., Kyrola, E., Auvinen, H., and Oikarinen, L.: An overview of the Odin atmospheric mission, Can. J. Phys., 80, 309–319, https://doi.org/10.1139/P01-157, 2002.

Ochiai, S., Baron, P., Nishibori, T., Irimajiri, Y., Uzawa, Y., Manabe, T., Maezawa, H., Mizuno, A., Nagahama, T., Sagawa, H., Suzuki, M., and Shiotani, M.: SMILES-2 Mission for Temperature, Wind, and Composition in the Whole Atmosphere, SOLA, 13A, 13–18, https://doi.org/10.2151/sola.13A-003, 2017.

Perrin, A., Puzzarini. C., Colmont, J.-M., Verdes, C., Wlodarczak, G., Cazzoli, G., Buehler, S., Flaud, J.-M., and Demaison, J.: Molecular Line Parameters for the "MASTER" (Millimeter Wave Acquisitions for Stratosphere/Troposphere Exchange Research) Database, J. Atmos. Chem, 51, 161-205, https://doi.org/10.1007/s10874-005-7185-9, 2005.

Pickett, H. M., Poynter, R. L., Cohen, E. A., Delitsky, M. L., Pearson, J. C., and Muller, H. S. P.: Submillimeter, millimeter, and microwave spectral line catalog, J. Quant. Spectrosc. Ra., 60, 883–890, https://doi.org/10.1016/S0022-4073(98)00091-0, 1998.

Pumphrey, H. C., Santee, M. L., Livesey, N. J., Schwartz, M. J., and Read, W. G.: Microwave Limb Sounder observations of biomass-burning products from the Australian bush fires of February 2009, Atmos. Chem. Phys., 11, 6285-6296, https://doi.org/10.5194/acp-11-6285-2011, 2011.

Pumphrey, H. C., Read, W. G., Livesey, N. J., and Yang, K.: Observations of volcanic SO_2 from MLS on Aura, Atmos. Meas. Tech., 8, 195-209, https://doi.org/10.5194/amt-8-195-2015, 2015.

Rodgers, C. D.: Inverse Methods for Atmospheric Sounding: Theory and Practice, World Scientific, Singapore, 2000.

Rothman, L. S., Gordon, I. E., Babikov, Y., Barbe, A., ChrisBenner, D., Bernath, P. F., Birk, M., Bizzocchi, L., Boudon,V., Brown, L. R., Campargue, A., Chance, K., Cohen, E. A., Coudert, L. H., Devi, V. M., Drouin, B. J., Fayt, A., Flaud,J.-M., Gamache, R. R., Harrison, J. J., Hartmann, J. -M., Hill, C., Hodges, J. T., Jacquemart, D., Jolly, A., Lamouroux, J., Le Roy, R. J., Li, G., Long, D. A., Lyulin, O. M., Mackie, C. J., Massie, S. T., Mikhailenko, S., Müller, H. S. P., Nau-menko, O. V., Nikitin, A. V., Orphal, J., Perevalov, V., Per-rin, A., Polovtseva, E. R., Richard, C., Smith, M. A. H., Starikova, E., Sung, K., Tashkun, S., Tennyson, J., Toon, G. C., Tyuterev, V. G., and Wagner, G.: The HITRAN2012 molecular spectroscopic database, J. Quant. Spectrosc. Ra., 130, 4–50, https://doi.org/10.1016/j.jqsrt.2013.07.002, 2013.

Santee, M. L., Lambert, A., Read, W. G., Livesey, N. J., Manney, G. L., Cofield, R. E., Cuddy, D. T., Daffer, W. H., Drouin, B. J., Froidevaux, L., Fuller, R. A., Jarnot, R. F., Knosp, B. W., Perun, V. S., Snyder, W. V., Stek, P. C., Thurstans, R. P., Wagner, P. A., Waters, J. W., Connor, B., Urban, J., Murtagh, D., Ricaud, P., Barrett, B., Kleinböhl, A., Kuttippurath, J., Küllmann, H., von Hobe, M., Toon, G. C., and Stachnik, R. A.: Validation of the Aura Microwave Limb Sounder ClO measurements, J. Geophys. Res.-Atmos., 113, D15S22, https://doi.org/10.1029/2007JD008762, 2008.

Sato, T. O., Sagawa, H., Kreyling, D., Manabe, T., Ochiai, S., Kikuchi, K., Baron, P., Mendrok, J., Urban, J., Murtagh, D., Yasui, M., and Kasai, Y.: Strato-mesospheric ClO observations by SMILES: error analysis and diurnal variation, Atmos. Meas. Tech., 5, 2809-2825, https://doi.org/10.5194/amt-5-2809-2012, 2012.

Schwartz, M. J., Read, W. G., Snyder, W. V.: EOS MLS forward model polarized radiative transfer for Zeeman-split oxygen, IEEE T. Geosci. Remote, 44, 1182-1191, https://doi.org/10.1109/TGRS.2005.862267, 2006.

Suzuki, M., Manago, N., Ozeki, H., Ochiai, S., and Baron, P.: Sensitivity study of smiles-2 for chemical species, in: Sensors, Systems, and Next-Generation Satellites XIX, Toulouse, France, 16 October 2015, 15, 2015.

Swadley, S. D., Poe, G. A., Bell, W., Hong, Y., Kunkee, D. B., McDermid, I. S., and Leblanc, T.: Analysis and Characterization of the SSMIS Upper Atmosphere Sounding Channel Measurements, IEEE T. Geosci. Remote, 46, 962–983, https://doi.org/10.1109/TGRS.2008.916980, 2008.

Takahashi, C., Ochiai, S., and Suzuki, M.: Operational retrieval algorithms for JEM/SMILES level 2 data processing system, J. Quant. Spectrosc. Ra., 111, 160–173, https://doi.org/10.1016/j.jqsrt.2009.06.005, 2010.

Takahashi, C., Suzuki, M., Mitsuda, C., Ochiai, S., Manago, N., Hayashi, H., Iwata, Y., Imai, K., Sano, T., Takayanagi, M., and Shiotani, M.: Capability for ozone high-precision retrieval on JEM/SMILES observation, Adv. Space Res., 48, 1076–1085, https://doi.org/10.1016/j.asr.2011.04.038, 2011.

Urban, J.: Optimal sub-millimeter bands for passive limb observations of stratospheric HBr, BrO, HOCl, and HO_2 from space, J. Quant. Spectrosc. Ra., 76, 145–178, https://doi.org/10.1016/s0022-4073(02)00051-1, 2003.

Urban, J., Baron, P., Lautié, N., Schneider, N., Dassas, K., Ricaud, P., and De la Nöe, J.: Moliere (v5): a versatile forward- and inversion model for the millimeter and sub-millimeter wavelength range, J. Quant. Spectrosc. Ra., 83, 529–554, https://doi.org/10.1016/S0022-4073(03)00104-3, 2004.

Urban, J., Lautié, N., Le Flochmoën, E., Jiménez, C., Eriksson, P., de la Nöe, J., Dupuy, E., Ekström, M., El Amraoui, L., Frisk, U., Murtagh, D., Olberg, M., and Ricaud, P.: Odin/SMR limb observations of stratospheric trace gases: Level 2 processing of ClO, N_2O, HNO_3, and O_3, J. Geophys. Res.-Atmos., 110, D14307, https://doi.org/10.1029/2004JD005741, 2005.

Waters, J. W., Froidevaux, L., Read, W. G., Manney, G. L., Elson, L. S., Flower, D. A., Jarnot, R. F., and Harwood, R. S.: Stratospheric ClO and ozone from the Microwave Limb Sounder on the Upper Atmosphere Research Satellite, Nature, 362, 597–602, https://doi.org/10.1038/362597a0, 1993.

Waters, J. W., Read, W. G., Froidevaux, L., Jarnot, R. F., Cofield, R. E., Flower, D. A., Lau, G. K., Pickett, H. M., Santee, M. L., Wu, D. L., Boyles, M. A., Burke, J. R., Lay, R. R., Loo, M. S., Livesey, N. J., Lungu, T. A., Manney, G. L., Nakamura, L. L., Perun, V. S., Ridenoure, B. P., Shippony, Z., Siegel, P. H., Thurstans, R. P.: The UARS and EOS microwave limb sounder experiments, J. Atmos. Sci., 56, 194–218, https://doi.org/10.1175/1520-0469(1999)056<0194:tuaeml>2.0.co;2, 1999.

Waters, J.W., Froidevaux, L., Jarnot, R.F., Read, W.G., Pickett, H.M., Harwood, R.S., Cofield, R.E., Filipiak, M. J., Flower, D. A., Livesey, N. J., Manney, G. L., Pumphrey, H. C., Santee, M. L., Siegel, P. H., and Wu, D. L.: An Overview of the EOS MLS Experiment., Tech. Rep. JPL D-15745 / CL# 04-2323, Jet Propulsion Laboratory, California Institute of Technology, Pasadena, California, 91109-8099, available at: https://mls.jpl.nasa.gov/data/eos_overview_atbd.pdf (last access: 26 March 2019), Version 2.0, 2004.

Waters, J. W., Froidevaux, L., Harwood, R. S., Jarnot, R. F., Pickett, H. M., Read, W. G., Siegel, P. H., Cofield, R. E., Filipiak, M. J., Flower, D. A., Holden, J. R., Lau, G. K., Livesey, N. J., Manney, G. L., Pumphrey, H. C., Santee, M. L., Wu, D. L., Cuddy, D. T., Lay, R. R., Loo, M. S., Perun, V. S., Schwartz, M. J., Stek, P. C., Thurstans, R. P., Boyles, M. A., Chandra, K. M., Chavez, M. C., Chen, G.-S., Chudasama, B. V., Dodge, R., Fuller, R. A., Girard, M. A., Jiang, J. H., Jiang, Y., Knosp, B. W., LaBelle, R. C., Lam, J. C., Lee, K. A., Miller, D., Oswald, J. E., Patel, N. C., Pukala, D. M., Quintero, O., Scaff, D. M., Snyder, W. V., Tope, M. C., Wagner, P. A., and Walch, M. J.: The Earth Observing System Microwave Limb Sounder (EOS MLS) on the Aura Satellite, IEEE T. Geosci. Remote, 44, 1075–1092, https://doi.org/10.1109/TGRS.2006.873771, 2006.

Wu, D. L., Schwartz, M. J., Waters, J. W., Limpasuvan, V., Wu, Q., and Killeen, T. L.: Mesospheric doppler wind measurements from Aura Microwave Limb Sounder (MLS), Adv. Space Res., 42, 1246–1252, https://doi.org/10.1016/j.asr.2007.06.014, 2008.